THESIS FOR THE DEGREE OF DOCTOR OF PHILOSOPHY

Microcapsules for Functionalization of Fibrous Materials

From Formulation Development to Long-term Microbial Infection Control

VIKTOR ERIKSSON

Department of Chemistry and Chemical Engineering
Chalmers University of Technology
Gothenburg, Sweden, 2023

Microcapsules for Functionalization of Fibrous Materials
From Formulation Development to Long-term Microbial Infection Control
VIKTOR ERIKSSON
ISBN 978-91-7905-962-0

Doktorsavhandlingar vid Chalmers tekniska högskola
Ny serie nr 5428
ISSN 0346-718X

Department of Chemistry and Chemical Engineering
Chalmers University of Technology
SE-412 96 Gothenburg
Sweden
Telephone: +46 (0)31 772 1000

Cover: An illustration visualizing the developed fiber spinning process for producing microcapsule-functionalized and biobased polysaccharide fibers.

Printed by Chalmers Digitaltryck
Gothenburg, Sweden, 2023

Microcapsules for Functionalization of Fibrous Materials
From Formulation Development to Long-term Microbial Infection Control
VIKTOR ERIKSSON
Department of Chemistry and Chemical Engineering
Chalmers University of Technology

Abstract

In response to growing concerns regarding the impact of antimicrobial agents on the environment and public health, a more sustainable approach to their use in products is needed. The problem originates from rapid and uncontrolled release, leading to difficulties in maintaining long-term efficacy. A common solution to prolong the lifetimes of materials is to increase the dose of active substances, however, this causes significant losses, pollution, and antimicrobial resistance development in microorganisms. A more sustainable solution would be materials that release these substances in a controlled manner, only slightly surpassing effective concentrations.

This thesis explores the utilization of microcapsule functionalization as a means of enabling a controlled release of active substances from fibrous materials. Successful control requires (*i*) a toolbox for tuning the release profiles from microcapsules and (*ii*) an effective functionalization strategy that retains the release rate-limiting properties of the microcapsules in the fibrous material. An improved theory for microcapsule morphology prediction following internal phase separation was first established, incorporating the importance of both thermodynamically controlled intermediate morphologies and the kinetics of formation. This allowed for improved morphology control during formulation, facilitating the development of microcapsule formulations capable of achieving both immediate release in response to pH changes and UV light exposure, as well as sustained long-term release over several weeks to months. A method for functionalizing wet-spun and solution-blown biobased polysaccharide fibers with these microcapsules was consequently developed and evaluated. The microcapsules were embedded within the fibers, retaining their rate-limiting properties and demonstrating the potential for creating a macroscopic controlled release material.

As a proof of concept, a prototype material was evaluated for long-term microbial infection control. In this material, microcapsules loaded with the antimicrobial agent octenidine dihydrochloride (OCT) were incorporated into a cellulose nonwoven textile. In vitro experiments confirmed that the sustained OCT release from the material prototype effectively provided long-term infection control against *S. aureus* for more than one week. In contrast, a control material loaded using conventional impregnation lost its antimicrobial efficacy after just 30 minutes. This highlights the possibilities associated with controlled release of actives, not only for infection control but also a wider range of applications.

Keywords: Microencapsulation, controlled release, antimicrobial.

List of Publications

This thesis is based on the work contained in the following appended papers:

I. A Unified Thermodynamic and Kinetic Approach for Prediction of Microcapsule Morphologies
Viktor Eriksson, Sofia Edegran, Matilda Croy, Lars Evenäs, and Markus Andersson Trojer
Submitted

II. Polyanhydride Microcapsules Exhibiting a Sharp pH-transition at Physiological Conditions for Instantaneous Triggered Release
Viktor Eriksson, Leyla Beckerman, Erik Aerts, Markus Andersson Trojer, and Lars Evenäs
Accepted for publication in Langmuir

III. Formulation of Polyphthalaldehyde Microcapsules for Immediate UV-light Triggered Release
Viktor Eriksson, Markus Andersson Trojer, Szilvia Vavra, Mats Hulander, and Lars Nordstierna
Journal of Colloid and Interface Science 579 (2020): 645-653

IV. Electrostatically Hindered Diffusion for Predictable Release of Encapsulated Cationic Antimicrobials
Viktor Eriksson, Erik Nygren, Romain Bordes, Lars Evenäs, and Markus Andersson Trojer
Submitted

V. Solution-spinning of a Collection of Micro- and Nanocarrier-functionalized Polysaccharide Fibers
Hanna Ulmefors, Ting Yang Nilsson, Viktor Eriksson, Gustav Eriksson, Lars Evenäs, and Markus Andersson Trojer
Macromolecular Materials and Engineering 307 (2022): 2200110

VI. Microcapsule Functionalization Enables Rate-determining Release from Cellulose Nonwovens for Long-term Performance
Viktor Eriksson, Jules Mistral, Ting Yang Nilsson, Markus Andersson Trojer, and Lars Evenäs
Journal of Materials Chemistry B 11 (2023): 2693-2699

VII. Microencapsulation as a Means for Resource-efficient and Long-term Infection Control: Antimicrobial Efficiency of and Sustained Release from Cellulosic Nonwovens containing PLGA-encapsulated octenidine
Viktor Eriksson, Lucia Gonzales Strömberg, Ingela Persson, Unn Tjörnstrand, Petter Melin, Frida Book, Britt Wassmur, Thomas Backhaus, Erik Nygren, Lars Evenäs, and Markus Andersson Trojer
Manuscript

My Contributions to the Publications

I. Main author. Supervised and participated in all experimental work and data analysis, except NMR studies.

II. Main author. Supervised and participated in the experimental work, performed in situ microscopy studies of degradation and most data analysis.

III. Main author. Responsible for all experimental work, except SEM and the degradation study by IR spectroscopy.

IV. Main author. Responsible for all experimental work and most data analysis.

V. Co-author. Responsible for parts of the microcapsule formulation and preparation of cellulose-based fibers. Analyzed most materials by optical and fluorescence microscopy and measured the loading efficiencies.

VI. Main author. Supervised and participated in all experimental work and data analysis, except SEM and the cytotoxicity study.

VII. Main author. Developed and prepared the studied fiber materials, performed all structure characterization of the materials, and measured and modeled all release data.

Contents

1

Introduction

Combating the growth of unwanted (micro)organisms has been a concern for humanity throughout history. Records dating back almost 4,000 years show evidence of using natural products with inherent antimicrobial properties in wound care, even though the world of microorganisms was not yet known at the time, to reduce bacterial infection [1]. Records from the same time also show that attaching sheets of metals such as copper and lead to wooden ship hulls was known to protect from marine fouling organisms [2]. Since the beginning of the 20th century, increasingly potent active substances for (micro)organism growth control have been discovered and commercialized. Some discoveries have significantly improved our quality of life. Penicillin, discovered in the 1920s, revolutionized healthcare by providing a novel means to combat pathogenic bacteria [3]. Other discoveries have, however, been associated with severe adverse effects. One such example is tributyltin, which found an application in antifouling paint for ship hulls in the 1960s [4]. While being extremely efficient at preventing fouling caused by marine species, it is also highly toxic to many non-target aquatic species which led to the collapse of marine ecosystems [5] and a subsequent total ban on its usage. These contrasting examples highlight the importance of responsible and sustainable development to avoid unintended environmental and ecological consequences.

The discovery of effective biocidal substances has led to widespread use in products today. Consequently, there is an alarming overuse in applications ranging from agriculture and aquaculture to the healthcare sector. Focusing on antimicrobial substances, microorganisms are continuously exposed to sub-effective doses as a result of their broad use. This has been connected with inducing the development of antimicrobial resistance (AMR) in certain strains of microorganisms [6]. Today, it is estimated that such resistant strains of bacteria cause 700,000 deaths per year. Without intervention, this number could increase to 10 million deaths by year 2050 [7]. As highlighted in the European Commission Zero Pollution Action Plan 2021 [8], there is consequently a need to minimize the use of these active substances. This is vital not only for reducing AMR development but also due to concerns regarding

potentially synergistic effects of the complex cocktail of antimicrobial agents present in the environment that could increase their toxicity [9].

At the same time, the need and desire to control microbial growth remains constant. Simply reducing the loading of antimicrobial agents in commercial products relying on their release today would significantly shorten functional lifetimes. By extension, this would lead to unsustainable material use with a need to discard and replace the products more frequently. Enabling a long functional lifetime necessitates maintaining the concentration of active substance above a certain *effective concentration*. A common approach for achieving prolonged functional lifetimes is to simply increase the dose of active substance in the material. This action does slightly increase the functional lifetime, although it leads to extensive pollution since everything released beyond the effective concentration is simply lost. This is the origin of the problem of significant antimicrobial overuse, highlighting the balance required for sustainable and effective microbial growth control. Moreover, if the products are used beyond their functional lifetimes, antimicrobial agents are still released at low concentrations below the effective concentration which drives AMR development [6]. Instead, the preferable solution is one where the release rate can be tuned to precisely release the amount needed to maintain the effective concentration over a long time. This can be realized by designing a controlled release profile that is slow and sustained.

Microencapsulation, which emerged in the 1930s, has proven to be an excellent strategy for achieving controlled release of actives [10]. Micron-sized particles provide a barrier, often of polymeric nature, that adds two main functionalities. Firstly, they protect sensitive actives from their surroundings. Many modern antimicrobial agents are designed to be biodegradable as mitigation of the issues concerning pollution and non-target toxicity. However, this can also add a demand for protection during storage and prior to release from materials. Secondly, they act as a rate-limiting barrier for release. The release can be either slow and *sustained* [11], or *triggered* [12] to instantaneously release the entire dose in response to external stimuli. This means that the release can be precisely controlled both in terms of how fast the actives are released, and when they are released. By precisely controlling the release rate, the dose of actives could be decreased with maintained functionality as a consequence of decreased losses.

To enhance the widespread applicability of microcapsules, it is often necessary to immobilize them within a matrix, creating a macroscopic material that enables a controlled release rather than a dispersion in a liquid. This has previously been successfully employed, for instance in antifouling coatings, where dispersing the microcapsules in the wet paint formulation is relatively straightforward [13]. After drying, the microcapsules thus become embedded within the coating. Another growing product segment that could greatly benefit from microcapsule functionalization is functional fiber materials. This product segment has been the focus of this thesis. Here, applications in wound care are easily conceived for long-term delivery of for

example antimicrobial agents. Over the past decades, advanced wound dressings have been innovated and commercialized to facilitate wound healing. By further extending the functional antimicrobial lifetime of these wound dressings, both patient discomfort and labor costs associated with dressing changes could be reduced. Products such as implants and materials for tissue engineering, as well as textiles for agriculture or aquaculture, are additional applications where microcapsule-functionalized textiles could add additional benefits [14].

Finally, the emphasis is not solely on enhancing product performance but also on doing so in a sustainable manner. In the case of fibrous materials, there is an increasing desire to replace fossil-based raw materials with bio-based, renewable, and biodegradable alternatives. Currently, synthetic fibers constitute 66% of the total market share in fiber production, while biobased regenerated fibers account for just 6% [15]. Given the abundance of cellulose as a feedstock [16] there exists significant potential for advancing the production of high-performance biobased textiles.

1.1 Purpose and Objectives

In this work, a versatile concept for microcapsule-functionalization of fibrous materials has been developed. To demonstrate a working example of the developed material concept, an application in wound care with the purpose of long-term infection control was studied. Consequently, functionalization to enable a controlled release of an antimicrobial agent has been the main focus of this work. To reach the desired release rate of actives, a variety of controlled release strategies in combination may be required. Initially, a sufficiently large dose needs to be rapidly released to reach effective concentrations. Following this, a slow and sustained release is required to maintain long-term efficacy. To obtain this desired release profile by microencapsulation, different formulations must be developed to work in unison. An initially triggered release formulation can rapidly increase the concentration of actives above the effective concentration upon exposure to external stimuli. A sustained release formulation can then maintain the concentration above the effective concentration to enable a long-term effect.

The objectives of this work were therefore divided into three parts: (*i*) developing a toolbox of different controlled release profiles from microcapsules, (*ii*) creating a macroscopic biobased material with an effective microcapsule functionalization, and (*iii*) evaluating the material concept in vitro for long-term infection control.

(*i*) In Paper I the microcapsule formulation itself was studied, identifying key parameters for control of the microcapsule morphology. With this knowledge, microcapsules capable of an instantaneous triggered release upon exposure to pH changes and light stimuli, respectively, were formulated in Paper II and Paper III. A subsequent sustained

release formulation was then developed for a slow and continuous release of a cationic antimicrobial agent in Paper IV. For all of these microcapsule systems, the mechanisms responsible for both a successful encapsulation and release were identified. Release models were also developed to describe the release and enable a *predictable* release.

(*ii*) A range of different fibers made from biobased polysaccharides and functionalized with microcapsules were developed in Paper V. The rate limiting release of a model substance from cellulose-based microcapsule-functionalized nonwovens was studied in Paper VI.

(*iii*) Finally, by functionalizing the materials prepared in Paper V with the antimicrobial-loaded microcapsules from Paper IV, the sustained antimicrobial effect of this material was evaluated in Paper VII.

2

Functionalized Textile Materials

The growing product segment of high-performance functionalized textiles utilizes functionalities beyond traditional decorative or protective properties. A wide range of these functionalized textile materials have been innovated for a variety of applications, such as scented or thermoregulating fibers [17]. For natural fibers such as cotton, common functionalization methods involve applying a surface coating or modifying the fiber's chemical structure [18, 19]. While adding versatility in the functionalization, such coatings on fibers can suffer from inadequate mechanical strength and long-term stability [20]. This leads to the search for alternative functionalization strategies. Greater functionalization freedom can be granted for regenerated or synthetic fibers via the ability to employ complex spinning techniques, such as producing fibers with a core-sheath morphology [21].

Focusing on functional textiles providing a controlled release of active substances, microcapsule functionalization is a promising avenue for providing versatile release properties. By making the microcapsules in a composite fibrous material entirely release rate-determining, the release properties of the microcapsules can be completely decoupled from the fiber matrix. This allows for significantly improved predictability of the release properties. Altering the release rate of such a system only requires modifications to the microcapsule formulation, not the macroscopic fiber matrix itself. Recent work on microcapsule functionalization is limited and has mainly involved various surface post-treatments of already prepared fibrous materials [22, 23] with the issues and limitations described above.

Colloid electrospinning has previously been investigated for producing nonwoven fibrous materials* functionalized with both organic and inorganic nanoparticles dispersed in the fiber bulk [24]. However, the release from these nanoparticles is generally faster than from microcapsules due to shorter diffusional pathways. This is especially true for inorganic

*Nonwovens are fibrous materials where the individual fibers are for example physically entangled or chemically bonded, resulting in a random three-dimensional fiber orientation as compared to the structured orientation of woven or knitted materials.

nanoparticles, such as mesoporous silica nanoparticles, where the actives are only adsorbed to the surfaces of the porous particles. For such a case, the nanoparticles can delay the release slightly but not act as a truly rate-limiting step. In this work, microcapsule functionalization of the fiber bulk was instead developed due to the superior release rate-limiting properties of microcapsules.

2.1 Antimicrobial Wound Dressings

When the skin is injured, a cascade of biological processes is set in motion. Initially, the focus is on stopping bleeding, followed by an inflammatory phase that helps remove pathogens. The third stage involves the formation of a new matrix to cover and start rebuilding the wound. In the final stage, this rapidly formed matrix undergoes remodeling and strengthening [25]. However, this progression can be disturbed in certain wounds. A so-called chronic wound remains in the inflammatory phase and does not progress to the subsequent proliferation phase [26]. Several risk factors contribute to the prevalence of chronic wounds, including conditions such as diabetes mellitus, as well as factors such as aging, overweight, and smoking [27]. However, our current understanding of the intricate processes that drive the transition from inflammation to proliferation in chronic wound healing remains limited. This poses a significant challenge in achieving successful healing within today's healthcare sector.

One well-established factor for the successful healing of chronic wounds is preventing microbial colonization [28]. All wounds, especially those showing delayed healing, are prone to microbial infection and bacterial biofilms can be found in most chronic wounds [29]. Hence, strategies for controlling microbial growth are essential in wound care products aimed at chronic or other hard-to-heal wounds. In commercially available products, several solutions to infection control can be found. The most common involves impregnating the wound dressings with antimicrobial agents, for example silver salts [30], that are subsequently released into the wound bed. However, this approach often lacks control over the release rate of antimicrobial agents, making it challenging to predict and manage their functional lifetimes and potentially resulting in ambiguous efficacy. Concerns have also been raised regarding the development of microbial resistance and potentially toxic side effects associated with common antimicrobial agents, such as silver [31, 32]. To avoid resistance development, alternate solutions relying on for example hydrophobic coatings that bind and immobilize microorganisms [33] have been commercialized, but their efficacy has also recently been questioned [34].

New strategies are therefore required for infection control in chronic wounds, both in terms of the choice of active substance and how a successful functionalization of the fibrous material in a wound dressing can be achieved. Cationic antimicrobial agents, such as quaternary ammonium compounds (QACs) [35], are one group of possible alternative substances. Despite being in use

for almost a century, the mechanism by which QACs exert their antimicrobial effect is not fully understood. However, it is based on electrostatic interaction between the cationic QAC and anionic phospholipids in the bacterial cell envelope. The QACs, often amphiphilic in nature, integrate into and disrupt the membrane, causing cell lysis [36, 37]. Common formulations of QACs today are aqueous solutions used as surface disinfectants, an application that became increasingly important during the COVID-19 pandemic.

In the development of QAC-functionalized antimicrobial materials, two main inactivation mechanisms are being studied: contact-killing and release-killing [38]. Contact-killing materials are substrates that are surface-functionalized with molecules bearing quaternary ammonium groups [39]. This approach has gained popularity due to the potential to enable long-term protection since it does not rely on the release of a finite amount of the antimicrobial agent. Instead, the antimicrobial effect is exerted once the colonizing microorganisms come within close proximity of the fiber surface. However, as a result of this, its effect may be limited in deep wounds and against bacterial biofilms. Additionally, fouling caused by the adhesion of microorganisms or solutes in wound exudate onto the functionalized surface must be minimized to maintain the antibacterial effect [40].

On the other hand, release-killing materials rely on releasing a sufficient amount of antimicrobial agent into the wound bed to exceed a certain *effective concentration*. Ideally, this effective concentration is only slightly exceeded over the entire functional lifetime to minimize losses. A potent antimicrobial agent with a low effective concentration, coupled with a slow and controlled sustained release, offers the potential for long-lasting antimicrobial protection without the fouling-associated risks of contact-killing surfaces. Octenidine dihydrochloride (OCT) is one such effective cationic antimicrobial agent [41] used in Paper IV and Paper VII. This substance displays a broad-spectrum activity with effective concentrations in the range of milligrams per liter against both gram-positive and gram-negative bacteria [42, 43].

2.2 Release Profiles

Maintaining a bulk concentration (c_b) above the effective concentration in the bulk of for example the exudate of a wound bed using a release-killing material involves a mass balance between two processes: the controlled release of the active substance ($\dot{m}_\mathrm{in}$) and its removal through processes like sorption into the body or uptake by microorganisms ($\dot{m}_\mathrm{out}$). This concept is illustrated schematically for a piece of nonwoven material immersed in a liquid volume containing bacteria in Figure 2.1. The net flux $\dot{m}(t)$ can in such an

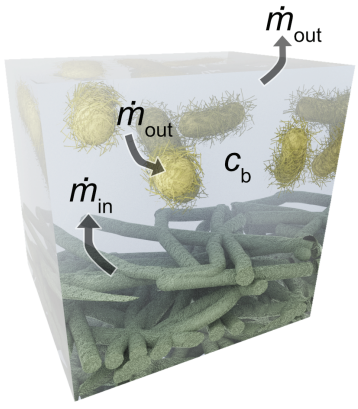

Figure 2.1: Piece of nonwoven material in a liquid volume containing bacteria.

example be expressed as

$$\dot{m}(t) = \dot{m}_{\text{in}}(t) - \dot{m}_{\text{out}}(t). \tag{2.1}$$

Assuming a constant $\dot{m}_{\text{out}}(t)$, a critical surface flux from the controlled release material can be defined below which the effective concentration is no longer maintained. This is illustrated in Figure 2.2a for two different cases of uncontrolled and controlled release, respectively. Anything released above the critical surface flux (shaded in green in Figure 2.2a) is, however, simply lost and may be potentially harmful. The point at which the flux falls below the critical flux defines the functional lifetime of the material (shaded in red in Figure 2.2a). Beyond this point, the antimicrobial efficacy is lost. Additionally, this is the region where the additional risk of driving antimicrobial resistance becomes significant [6, 44].

In practice, release is typically measured and expressed as the cumulative released amount,

$$m(t) = \int_0^t \dot{m}(t)dt, \tag{2.2}$$

and normalized to the total loading m_{tot} to yield a fractional (cumulative) release $m(t)/m_{\text{tot}}$. The release profiles corresponding to those in Figure 2.2a are expressed based on their fractional release in Figure 2.2b. Also note the conversion to a logarithmic time axis in Figure 2.2b to capture release events both on the time scale of seconds and days or months.

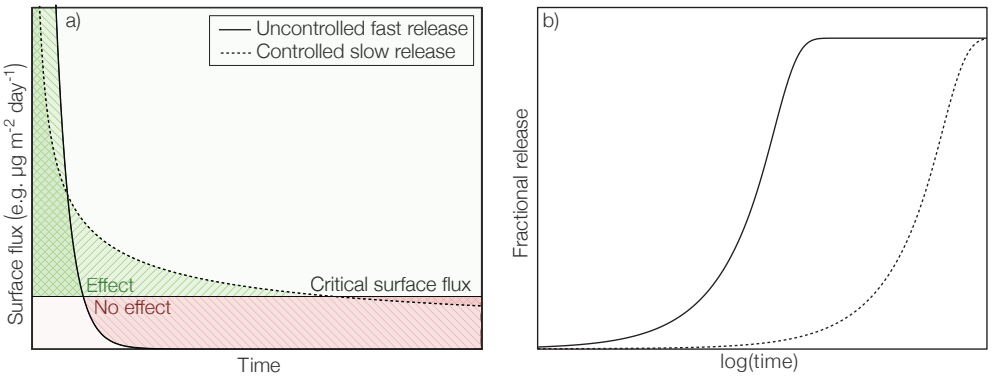

Figure 2.2: Release of an active substance from a material expressed in terms of a) flux at the material's surface and b) amount released into a bulk medium. Only above the critical surface flux is the antimicrobial effect maintained as shown in green. The legend is valid for both subfigures.

3

Microcapsule Formulation

One of the first large-scale commercial applications of microcapsules for controlled release of actives was carbonless copy paper in the 1950s, where a dye was encapsulated and its release triggered by mechanical force upon use. Today, one of the most common applications is the controlled delivery of pharmaceuticals, where the formulations are tailored to enable desirable and predictable release profiles [45–47]. Other applications of relevance for microcapsule formulations are e.g. antifouling [48] and self-healing [49, 50] coatings, food additives [51], and antimicrobial wound dressings [52]. The use of microcapsules is, however, not limited to the controlled release of actives. They can also be used to protect the encapsulated actives from their surroundings or confine them in space for applications like electronic paper displays [53], sensors [54] and microreactors [55].

There is not only a wide range of applications for microcapsules but also a wide range of methods for their formulation. Focusing on microcapsules with polymeric shells, which is the only type considered in this thesis, there are two main categories into which these formulation routes can be divided: chemical and physical methods [56]. In the chemical methods, the microcapsule shell is formed in situ by e.g. interfacial polymerization of oil-in-water emulsions [10]. The physical methods instead rely on the use of pre-formed polymers, in processes based on for example coacervation of a polymer-rich phase or layer-by-layer assembly of polyelectrolytes.

Throughout this work, the process of internal phase separation by solvent evaporation has been employed for formulating microcapsules. This is a coacervation-based physical method for formulating microcapsules that was first developed by Loxley and Vincent [57]. In this thesis work, it has been used because of its robustness and versatility, allowing for precise control of the microcapsule shell thickness. Since the shell polymer is synthesized beforehand, it can be synthesized according to well-established protocols which results in an excellent control of the physicochemical properties of the microcapsule shell. Second, it can be used for encapsulating sensitive active substances. Following the chemical methods based on in situ polymerization, there is a risk of side reactions between reactive monomers and the

active substance occurring. On the other hand, the physical methods require the shell material to be dissolved in an appropriate solvent. This limits the applicability of e.g. crosslinked polymers that are routinely produced following interfacial polymerization [58]. Additionally, formulation by internal phase separation is most suitable for microcapsules with hydrophobic oil cores, although it has been expanded by Atkin et al. [59] for formulating aqueous core microcapsules. If aqueous core microcapsules are desired, alternate physical routes such as those based on multiple emulsifications are instead often preferred [60, 61].

3.1 Internal Phase Separation

The principle of formulating microcapsules following internal phase separation by solvent evaporation is shown schematically in Figure 3.1. Here, the shell and core materials of the microcapsules along with any active substances are initially dissolved in a volatile organic solvent (e.g. dichloromethane, chloroform, or ethyl acetate [62]). There are three main properties that the organic solvent must possess in this process: (*i*) a capability of molecularly dissolving all microcapsule components, (*ii*) a low aqueous solubility, and (*iii*) a sufficient volatility.

This formed oil phase is then dispersed into an aqueous phase containing a dispersant (for example poly(vinyl alcohol) or poly(methacrylic acid)) under high-speed shearing to form an oil-in-water emulsion. After dilution of the formed emulsion, it is left under gentle magnetic stirring for the volatile solvent to evaporate. During this process, the organic solvent is transported from the emulsion droplet via the aqueous phase to the air-water interface where evaporation occurs. Consequently, the evaporation rate is governed by both the aqueous

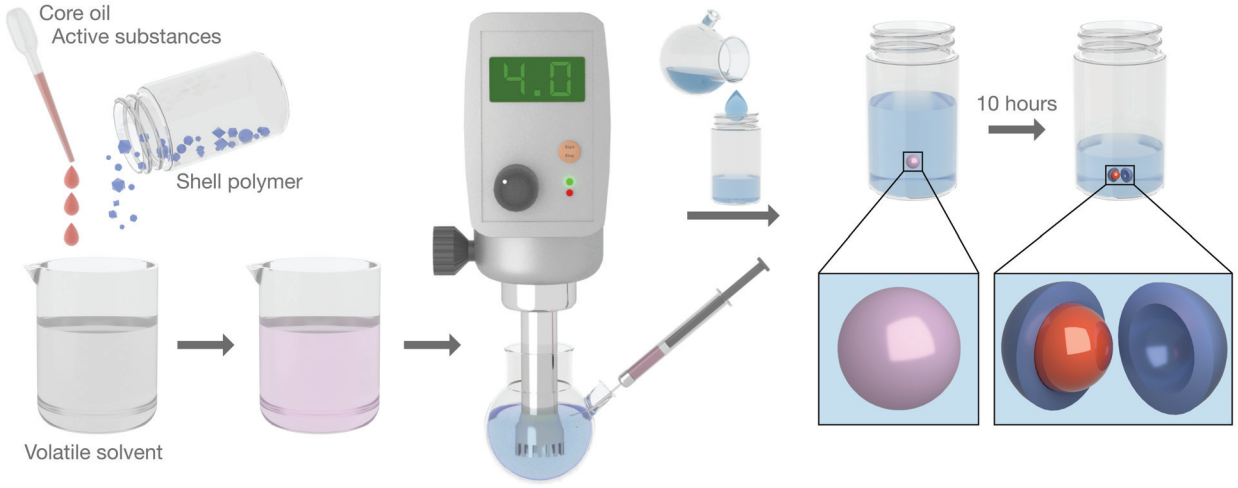

Figure 3.1: Schematic illustration of the formulation procedure for producing microcapsules.

solubility of the organic solvent* and the air-water surface area available for evaporation. As the volatile solvent evaporates, the organic phase inside the emulsion droplets will reach a point where internal phase separation occurs to form a two-phase system. If the microcapsule components are correctly balanced, as discussed later, the outcome will be microcapsules of core-shell morphology. By tuning the pressure at which the evaporation is performed, the evaporation rate can be further controlled. If the rate of evaporation is rapid, by e.g. rotary evaporation at reduced pressure, an increase in microporosity has previously been observed which led to an increased diffusivity and release rate of the encapsulated active [63]. The presented methodology can also be used in the formulation of monolithic microsphere particles, with the only modification being that the core material is replaced with an equal amount of shell material.

3.1.1 Morphologies

The internal phase separation process can result in a wide range of microparticle morphologies, some of which are presented in Figure 3.2. Focusing on the multicompartment microparticles, their formed morphology is determined by the strive to minimize the interfacial energies of the system. The wide range of possible morphologies thus calls for a model to predict the morphological outcome in a formulation of two or more mutually insoluble microcapsule components. Thermodynamical models for morphology prediction of microcapsules prepared by internal phase separation have been developed based on the spreading coefficients of the different phases. Torza and Mason [64] developed this concept for determining the morphologies in a system of three immiscible liquids. Both Sundberg et al. [65] as well as Loxley and Vincent [57] later expanded this concept further to also predict the morphologies in three-phase systems containing a solid polymer phase as in the case of a microcapsule. The spreading coefficient S_i for phase i in a system of three immiscible phases i, j, and k can be calculated from the three different interfacial tensions (γ_{ab}) between the phases in the system,

$$S_i = \gamma_{jk} - (\gamma_{ij} + \gamma_{ik}). \tag{3.1}$$

For a typical two-phase system, spreading coefficients for the following three phases must be considered: the oil phase (S_o), the aqueous phase (S_w), and the polymer phase (S_p). Four different conditions for these combinations of spreading coefficients can be defined, as shown by Equations 3.2 - 3.5, each predicting a discrete morphology.

$$S_o < 0; \quad S_w < 0; \quad S_p > 0 \tag{3.2}$$

$$S_o < 0; \quad S_w < 0; \quad S_p < 0 \tag{3.3}$$

$$S_o < 0; \quad S_w > 0; \quad S_p < 0 \tag{3.4}$$

$$S_o > 0; \quad S_w < 0; \quad S_p < 0 \tag{3.5}$$

*The aqueous solubility of dichloromethane is 18 g/L.

Only when the conditions in Equation 3.2 are fulfilled will the system adopt a core-shell morphology (Figure 3.2b). An acorn morphology (Figure 3.2c) will form if the conditions in Equation 3.3 are fulfilled, and the conditions in Equation 3.4 will lead to complete droplet separation (Figure 3.2d). If $\gamma_{ow} < \gamma_{pw}$ the conditions in Equation 3.5 can be fulfilled, leading to the formation of an inverted core-shell morphology (Figure 3.2e). In addition to these thermodynamically predicted morphologies, there are several other morphologies found in the literature, some of which are shown in Figure 3.2, that cannot be predicted by this model. As an example, both the blueberry and muticore microcapsules in Figure 3.2b1-b2 fall under the core-shell prediction, even though their morphologies are vastly different. As a consequence, several – occasionally conflicting – purely thermodynamic or pseudo-kinetic theories have been presented in the literature [66–68]. Recently, machine learning algorithms have also been developed to improve the accuracy of morphology prediction [69]. While increasing the accuracy of the prediction, those models based on machine learning often do not give a fundamental understanding of the factors affecting the formulation and morphological outcome. In Paper I, the thermodynamic model based on spreading coefficients described above was instead expanded by considering the entire microcapsule formation pathway. During the solvent evaporation process, the interfacial tensions are continuously changing as a result of the changing phase compositions. Rather than only considering the spreading coefficients of the final state, the entire formulation was considered by defining time-dependent spreading coefficients to introduce the kinetics of formation as a parameter of importance. This process and its evolution was further described by the formation pathway in a ternary system of the coacervating emulsion droplets.

It is important to note that the role of the polymer phase is significantly different in a monolithic microcapsule compared to a core-shell microcapsule. Consequently, the choice of morphology imparts its own requirements on the polymer phase. In monolithic microcapsules, accommodating a large amount of active dispersed in the polymer matrix is an important figure of merit. A high initial loading in the microcapsules leads to a more sustainable and resource-efficient material use. The opposite, i.e. a low solubility of the active in the polymer, is desired in the case of a core-shell particle to reduce the flux of the active through the shell. Combining this with a core where the solubility of the active is high leads to a case of both slow release and high encapsulation capacity.

3.1.2 Interfacial Tensions and the van Oss Formalism

To predict the morphologies of the formulated microcapsules, knowledge regarding the interfacial tensions of the system is required. Additionally, as hypothesized in Paper I, not only the final microcapsule state but also the interfacial tensions in its intermediate states during formation are important. The interfacial tension between two liquid phases can be readily measured directly by the pendant drop technique [70]. The curvature of a pendant droplet hanging from the tip of a needle depends on the interfacial tension between the droplet

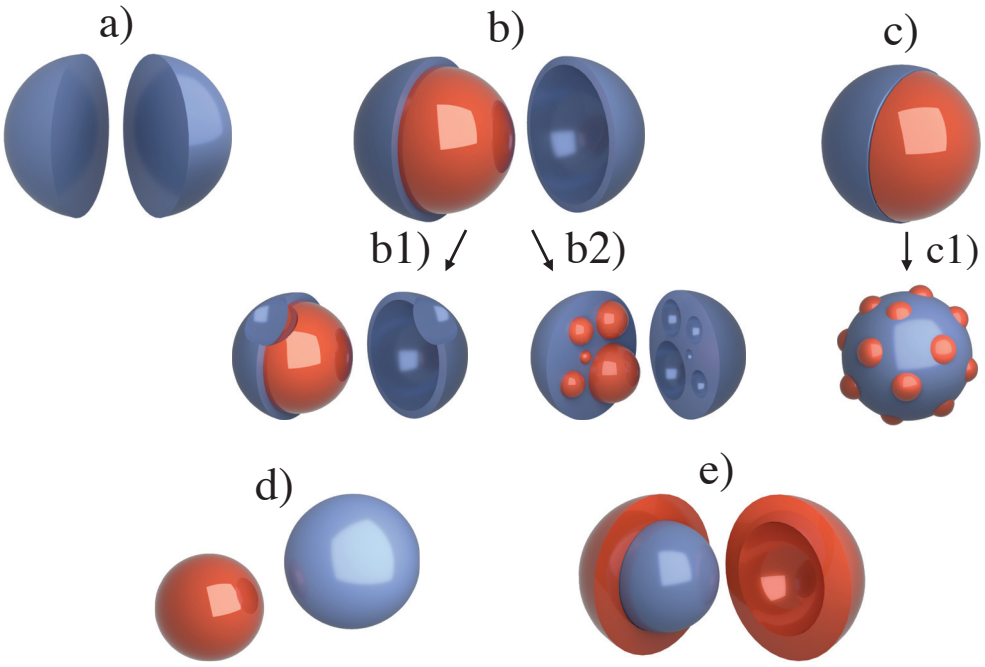

Figure 3.2: Schematic illustration of a selection of possible microparticle morphologies: a) homogeneous microsphere, b) core-shell particle, b1) *blueberry*-type particle and b2) multicore particle, c) *acorn* particle, c1) *raspberry*-type particle, d) complete droplet separation, and e) inverted core-shell. The solid polymer phase is represented in blue, and the liquid oil phase is shown in red.

and the surrounding medium, among other factors. The interfacial tension for such a pendant drop is defined as

$$\gamma = \frac{\Delta\rho g R_0}{\beta} \tag{3.6}$$

where $\Delta\rho$ is the density difference between the droplet and its surrounding medium, g is the gravitational acceleration, R_0 is the curvature radius at the droplet apex, and β is a shape factor.

The surface free energy of a solid polymer in contact with a liquid or gaseous phase cannot be measured directly. Instead, indirect methods are required. Van Oss and coworkers [71] developed a method for determining the surface energy of a solid polymer phase, based on measuring the contact angles of several well-known test liquids on the substrate of interest. Any surface tension or surface free energy (γ_i^{tot}) for a given liquid or solid i can be divided into Lifshitz-van der Waals (LW) and Lewis acid-base (AB) interactions, Equation 3.7. The acid-base interactions can be further divided into electron acceptor (γ_i^+) and electron donor (γ_i^-) interactions according to Equation 3.8. Following the formalism by van Oss, the contact angles (θ) of several known test liquids are measured on the studied solid substrate. By nonlinear regression, the polymer surface energy γ_S^{tot} can be determined through Equations 3.7 - 3.9. By finally measuring the contact angles of the liquids of interest on the

polymer surface, their interfacial tensions can be determined through Equation 3.10, knowing both the surface tension of the liquid of interest (γ_L^{tot}) and the surface energy of the polymer.

$$\gamma_i^{tot} = \gamma_i^{LW} + \gamma_i^{AB} \tag{3.7}$$

$$\gamma_i^{AB} = 2\sqrt{\gamma_i^+ \gamma_i^-} \tag{3.8}$$

$$1 + \cos(\theta)\gamma_L^{tot} = 2\left[\left(\gamma_S^{LW}\gamma_L^{LW}\right)^{1/2} + \left(\gamma_S^+\gamma_L^-\right)^{1/2} + \left(\gamma_S^-\gamma_L^+\right)^{1/2}\right] \tag{3.9}$$

$$\gamma_S^{tot} = \gamma_{SL} + \gamma_L^{tot}\cos(\theta) \tag{3.10}$$

3.2 Release Mechanisms

Following successful encapsulation into microcapsules of the desired morphology, there are several possible routes by which an encapsulated active can be released. Two main forms of controlled release exist as mentioned previously: triggered and sustained release. The microcapsules can be formulated to respond to external stimuli, giving the possibility of releasing all of the encapsulated material instantaneously in a controlled manner. Alternatively, the release can be slow and sustained, and controlled by for example a restricted and rate-limiting diffusivity of the actives through the microcapsule shell.

3.2.1 Stimuli-responsiveness

A plethora of stimuli-responsive microcapsules have been formulated that upon exposure to external stimuli release the encapsulated material. These triggering events include changes in pH or temperature and exposure to light of specific wavelengths among others [12]. Upon exposure to the stimulus, the most common release mechanism is an induced depolymerization of the microcapsule shell. However, a rapid release on the time-scale of seconds is more uncommon. In this thesis, two different polymeric shells – sensitive to pH-changes and UV-light, respectively – as shown in Figure 3.3a-b have been used for formulating core-shell microcapsules capable of achieving an instantaneous release of the encapsulated species.

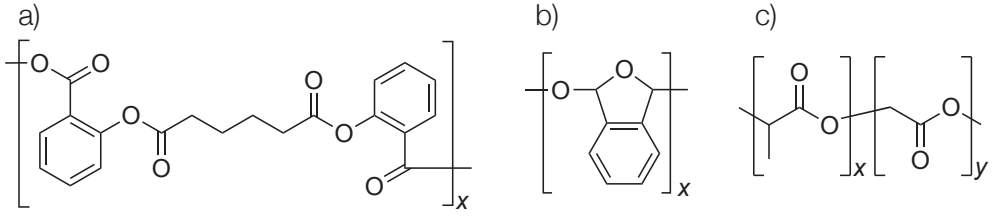

Figure 3.3: Molecular structures of a) poly(bis(2-carboxylphenyl)-adipate), b) polyphthalaldehyde, and c) poly(D,L-lactic-*co*-glycolic acid).

Polyanhydrides have gained significant attention for the delivery of actives [72–74]. Both aliphatic and aromatic repeating units have been employed as a tool to control properties such as the crystallinity, glass transition temperature, and hydrophobicity of the polymer. The poly(bis(2-carboxylphenyl)-adipate) shown in Figure 3.3a was developed by Uhrich and coworkers and its synthesis and properties have since then been extensively studied [75–78]. The polymer is highly pH-sensitive as a consequence of the presence of anhydride groups along the backbone that are readily hydrolyzed at alkaline pH. Utilizing this sensitivity, pH-responsive microcapsules were formulated in Paper II. The pH of healthy skin is normally slightly acidic, whereas it in chronic wounds normally is slightly alkaline [79, 80]. This shift in pH could be utilized as a basis for triggering the release of antimicrobial agents selectively in chronic wounds using poly(bis(2-carboxylphenyl)-adipate) microcapsules. Previously, this polyanhydride has mostly been used as the main component in macroscopic, millimeter-sized devices, such as implants [75, 81]. Because of their size, these devices typically degrade over a period of weeks to months. The original use of the polymer was as a depot for long-term delivery of the anti-inflammatory salicylic acid, one of the monomers in the repeating unit.

Polyphthalaldehyde (PPA, shown in Figure 3.3b) was first synthesized by Aso and Tagami in the 1960s [82], and it later found an application as a positive photoresist material in lithography [83, 84]. Its application in microencapsulation is, however, limited to only a handful of recent publications [66, 85, 86]. Here, either the inherent acid-sensitivity of polyphthalaldehyde or a fluoride-sensitive end cap has been utilized to trigger release. Upon chain scission or removal of the sensitive end-cap, the polymer rapidly reverts to its monomeric constituents. This is enabled by the low ceiling temperature[†] of polyphthalaldehyde of -40 °C [88]. In Paper III the UV light-sensitivity of polyphthalaldehyde was utilized. Using light to trigger release can have notable benefits as it does not necessitate altering the properties of the surrounding medium, such as pH or temperature. Consequently, this approach enables the potential for a fully remote triggering mechanism.

3.2.2 Diffusion and Erosion

Small molecules, such as biocides or antibacterial agents, readily diffuse within soft materials. In a dense polymer shell of a microcapsule, the diffusivity can be highly restricted and is controlled both by the free volume inside the polymer matrix as well as parameters like its porosity and tortuosity [11, 63]. This leads to slow diffusion-controlled mass transport of the encapsulated active, and consequently a sustained release. To further restrict the mass transport of hydrophobic actives from the microcapsules, surface modification by polyelectrolyte multilayer assemblies can be employed [13]. Despite a thickness on the nanometer scale, this highly charged and polar environment can drastically reduce the

[†]The temperature at which the depolymerization rate is equal to the polymerization rate, i.e., a measure of the tendency for the polymer to revert to its monomeric form [87].

permeability of actives and act as an additional release barrier. In Paper IV and Paper VII, specific interactions were instead utilized as a means of restricting the diffusivity further. An electrostatic binding between the active and microcapsule matrix led to a drastically restricted diffusivity within the microcapsule, and a significantly reduced release rate.

In addition to a diffusive release, erosion of the microcapsule may also cause a sustained release of encapsulated actives. Biobased aliphatic polyesters, such as poly(D,L-lactic-*co*-glycolic acid) (PLGA) in Figure 3.3c, have attracted popularity as microcapsule matrices in pharmaceutical settings [89, 90]. They are biodegradable by hydrolysis of the ester groups along the backbone, degrade into safe degradation products, and can be produced from renewable resources, all of which are attractive properties [91, 92].

Compared to the stimuli-responsive polymers described above, this hydrolytic degradation is significantly slower. By tuning the lactic-to-glycolic ratio and molecular weight of the polylactides, their hydrolytic degradation can be controlled on the time scale of weeks to several months [93]. A key property of the polylactide microcapsules is that they are hydrolyzed by bulk erosion due to significant swelling of the matrix by water [94]. As the matrix degrades, water-filled pores form inside the microcapsules. More carboxylate groups are progressively formed, leading to increasing acidity in the matrix which further catalyzes and increases the degradation rate in an autocatalytic manner [95]. This phenomenon and its implications on the release of actives has been studied further in detail by both Gu et al. [96] and Gasmi et al. [97] with the help of microscopic analysis of individual particles. In these systems, the release of actives is therefore not only limited by diffusion through the polymer matrix. The actives can additionally be released via diffusion through water-filled pores or osmosis-driven convection [93].

4

Exploring the Properties of Microcapsules and Fibers

Insight into the microscale world is a fundamental prerequisite to both microcapsule formulation and subsequent functionalization of fibers. In this section, the central analysis techniques employed in this work are presented. The morphology of microcapsules and the microstructure of fibrous materials are two of the most important puzzle pieces to describe the properties of the materials in this work. Consequently, accurate visualization is important, for which a range of microscopy techniques have been used. To further understand the encapsulation and controlled release of actives, specific interactions between the microcapsule matrix and the encapsulated active have been characterized using Fourier transform infrared spectroscopy.

Beyond characterization, understanding the release properties is crucial for assessing functionality. This section not only outlines the methodology for measuring release from both microcapsules and fibrous materials but also highlights key considerations for ensuring high-quality release data. Additionally, the introduction of release models facilitates improved material understanding from the extraction of parameters related to the release of actives, such as diffusivity or microcapsule degradation rate constants. This can in turn be used to predict and control the material's performance.

4.1 Morphology and Structure

Optical microscopy is a powerful tool for studying the morphology and microstructure of both microcapsules and fibrous materials. Unlike scanning electron microscopy, optical microscopy offers a non-invasive approach that allows for observations of specimens in their natural, often aqueous, environment. Consequently, any artifacts caused by sample preparation for analysis can be minimized. Moreover, microscopy allows for selective staining

using dyes (chromophores or fluorophores) that can aid in the identification of distinct phases, such as individual microcapsule compartments, within a sample.

4.1.1 Wide-field Microscopy

The simplest form of microscopy is performed by illuminating the entire sample with white light. Any light that is transmitted through the sample is magnified and focused by a combination of lenses, after which the transmitted image is recorded by a camera. To achieve an even illumination over the entire field of view and keep the light source out of the captured image, so-called Köhler illumination [98] was developed. Any attenuation by the sample gives rise to the observed contrast between a white background and a dark sample [99]. Hence, this technique is normally named brightfield microscopy.

A common problem with brightfield microscopy is the lack of contrast in several – especially biological – samples where the difference in refractive index between subject and background is low, which leads to low attenuation by the sample. Multiple approaches have been developed for improving this, such as the use of special contrast-enhancing techniques like differential interference contrast [99]. As the name suggests, it is based on the interference between two beams of light that pass through the sample. Before reaching the sample, the illuminating light is split into two beams of orthogonally polarized light that pass the sample within close proximity of each other. Any differences in refractive index or sample thickness encountered by the two beams will cause a phase shift. After passing the sample, the beams are recombined into the same polarization and any interference between them gives rise to the observed changes in intensity.

To further enhance the contrast or allow for differentiation between phases, fluorescent dyes may be used. This way, it is possible to selectively stain for example the core and shell of a microcapsule separately for structure elucidation [68]. To utilize fluorophores in a microscope, several modifications are required from the brightfield illumination described previously [99]. Rather than illuminating the sample with white light (the full visible wavelength spectrum), only a narrow interval of wavelengths is used and chosen to excite the selected fluorophore to higher energy levels. When the molecule returns to the ground state, light of a slightly longer wavelength can be emitted. This is the light that is observed and recorded in the microscope. Not all of the incident light is absorbed by the fluorophores and re-emitted as fluorescence. Parts of the excitation light may be scattered by the sample. In addition, not all of the light that is absorbed by the fluorophores gives rise to fluorescence. The *quantum yield* is defined as the ratio between the number of absorbed and emitted photons and gives a measure of the brightness of emission [100]. To only detect the emission light originating from the fluorophore, and not the much brighter reflected excitation light, a combination of filters is required so that only the emitted light is allowed to pass to the detector.

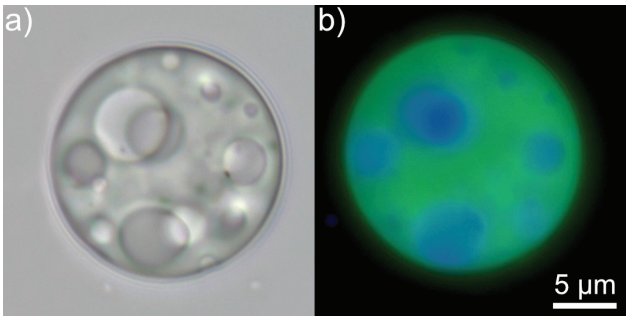

Figure 4.1: Micrographs of polyanhydride microcapsules from Paper II visualized by a) optical (brightfield illumination) and b) fluorescence microscopy. The scale bar is valid for both subfigures.

Figure 4.1 illustrates the characterization benefits of using fluorescence microscopy for the multicore polyanhydride microcapsules formulated and studied in Paper II. The shell-forming polyanhydride is autofluorescent (green) and the core has been stained with the hydrophobic substance pyrene (blue). This allows for detailed elucidation of complex – in this case multicore – microcapsule morphologies.

4.1.2 Confocal Laser Scanning Microscopy

A large amount of light is captured in wide-field microscopy, which leads to short acquisition times that are beneficial when for example studying moving objects. However, this can also result in poor contrast due to the collection of out-of-focus light. To address this issue, confocal laser scanning microscopy (CLSM) was developed [99]. By allowing the light to pass through a small pinhole before it reaches the detector, any out-of-focus light can be effectively filtered out. To generate a complete two-dimensional image, the light is scanned point by point across the image, and the intensity of emitted light from the focal plane at each point in the sample is recorded. Although CLSM is an inherently slower technique that requires more light, it offers increased contrast and resolution in the acquired images.

By only recording a thin slice of the sample, an additional possibility in structure visualization is given. Through the acquisition of two-dimensional images at multiple adjacent focal planes, these can be combined in post-processing to produce a three-dimensional representation of the sample. This is demonstrated in Figure 4.2 where a sample of microcapsule-loaded fibers is visualized both as a three-dimensional reconstruction and as orthogonal projections. To differentiate between microcapsules and fibers, the sample was stained with rhodamine (green) and methylene blue (red) to selectively stain the microcapsules and fibers, respectively. With the help of this technique, it is possible to determine for example the three-dimensional distribution of microcapsules in the entire fiber, and not only study the two-dimensional projection observed in a conventional fluorescence microscope.

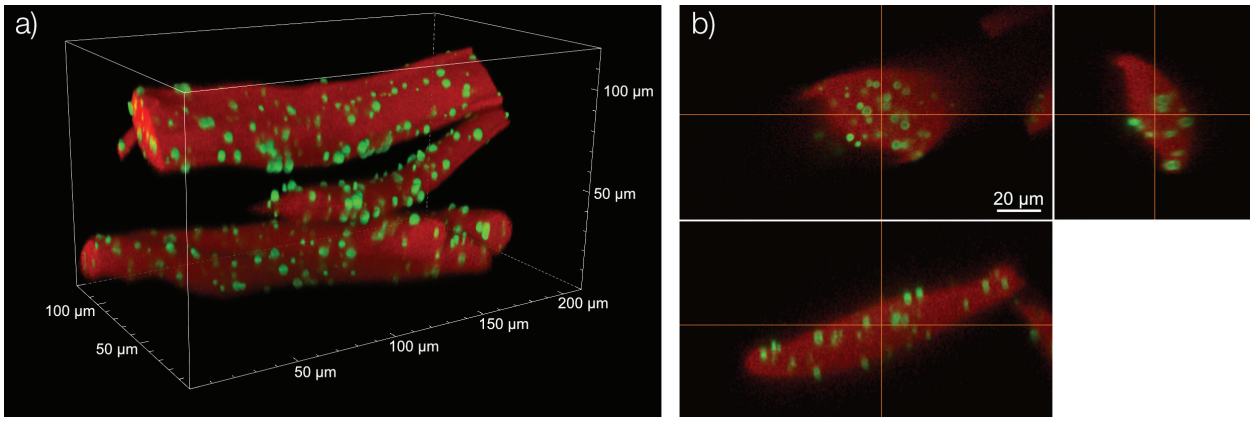

Figure 4.2: Stained microcapsule-loaded nonwoven material as visualized by CLSM. The entire three-dimensional volume was reconstructed as shown by a) three-dimensional volume rendering and b) orthogonal projections.

4.1.3 Size Distributions

Size is a key property that defines the release rate from a microcapsule or fibrous material as discussed in Section 4.3.2. Consequently, since both the formulated microcapsules and fibrous materials are polydisperse in size, accurately determining their size distributions is crucial. For the analysis of particles on the micrometer scale, laser diffraction analysis is commonly employed [101]. Such measurements are based on the principle that the angle of diffracted light is dependent on the particle size. The angular dependence of the diffracted light is measured, and through analysis with appropriate models this data can be converted to a size distribution of particles.

Comparatively large sample volumes on the orders of at least several milliliters are, however, required for this technique. Consequently, an image analysis technique based on optical micrographs was developed in this thesis, where individual microcapsules were counted and measured in an automatized manner. This reduced the required microcapsule sample volumes to tens of microliters. In addition to quantifying the polydispersity of the formulated microcapsules, this technique permitted analysing the polydispersity of fiber cross-sections in the studied nonwoven materials.

4.2 Specific Interactions Characterized by Infrared Spectroscopy

Attaining information on the molecular level about interactions between the microcapsule polymers and encapsulated actives can provide a basis for understanding the mechanisms behind encapsulation and release of actives. One useful tool for studying these interactions is Fourier transform infrared spectroscopy (FTIR). When molecules are exposed to infrared light, they absorb it at specific wavelengths corresponding to the excitation of vibrational modes between their atoms [102]. In a simple diatomic molecule, the vibrational frequency depends

on the bond strength and the mass of the two atoms. Intermolecular interactions will also affect the intramolecular vibrational frequencies and the absorbed wavelengths of light. By studying the shift of the wavenumbers of the absorption bands, phenomena such as electrostatic interaction can be identified [103, 104].

4.3 Release Measurements

The release rates of all systems in this thesis were measured in aqueous release media. To evaluate the release from microcapsules, a small volume of the prepared microcapsule suspension was mixed into a larger volume of aqueous release medium that was gently stirred using a magnetic stirrer. At specified intervals, aliquots were extracted and the microcapsules were separated from the continuous phase through filtration or centrifugation. The amount of active released at each point in time was determined by UV-visible spectrophotometry. The released amount $m(t)$ was related to the total loading m_{tot} by the fractional release $m(t)/m_{\text{tot}}$. The release from fibrous materials was measured in an analog manner by immersing a small piece of the fibrous material in the aqueous release medium.

To achieve high-quality release data, it is crucial to ensure sufficient solubility of the active substance in the aqueous phase. This is commonly referred to as satisfying *sink conditions*. Without this, the partitioning of the active between the release material (microcapsules, fibers, etc.) and the aqueous phase significantly affects the release pattern [105]. Additionally, accurately measuring very low concentrations of the released active can become challenging. For hydrophobic actives, such as pyrene used in this thesis, the aqueous solubility is very low and in the range of a few milligrams per liter. For such substances, solubilizing agents are commonly added to the aqueous phase to increase the solubility without otherwise affecting the system. In these studies, the nonionic surfactant Brij L23 ($C_{12}E_{23}$) was used for this purpose. Its hydrophilic-lipophilic balance (HLB) of 17 along with a low CMC of 0.01 wt.% makes it a suitable choice as a solubilizer. It is essential in these cases that the solubilizer for instance does not swell the polymer matrix of the microcapsules. This could impact the free volume of the polymer and consequently affect the rate-limiting diffusivity of the active.

4.3.1 UV-visible Spectrophotometry

A large number of molecules absorb light in the ultraviolet to visible range, making UV-visible spectrophotometry a common, simple, and convenient approach for both qualitative and quantitative analysis of chemicals. From the Beer-Lambert law, Equation 4.1, a linear relationship is established between absorbance (A) and concentration (c).

$$A = \log_{10}\left(\frac{I_0}{I}\right) = \varepsilon c l \tag{4.1}$$

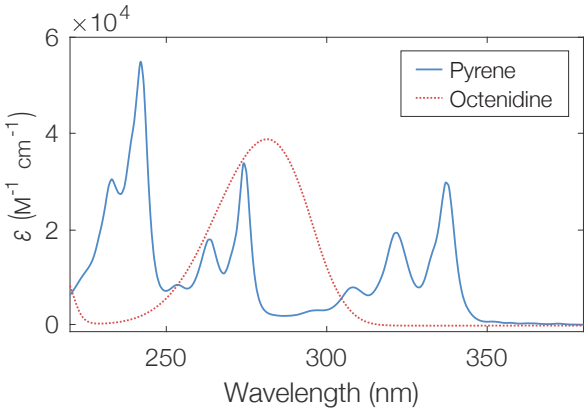

Figure 4.3: UV-vis absorption spectra of pyrene and octenidine dihydrochloride expressed based on their molar absorptivities (ε) in an aqueous 0.5 wt.% Brij L23 solution.

Here, I_0 and I are the intensities of the incident and transmitted light through the solution, respectively, ε is the (wavelength-dependent) molar absorption coefficient, and l is the path length through the solution. Both of the active substances studied in this thesis, pyrene and octenidine dihydrochloride, absorb ultraviolet light with absorption spectra shown in Figure 4.3.

4.3.2 Release Models

Several empirical or semi-analytical models can be found in the literature to describe the release from microcapsules. However, the validity of many of these models is dependent on achieving sink conditions. By instead describing the diffusion-controlled release of a small molecule from a matrix by the analytical solution to the diffusion equation, any partitioning between the matrix and release medium can be accounted for, thus eliminating the requirement of perfect sink conditions. In its simplest form, the equation can be reduced to a one-dimensional problem, expressed as

$$\frac{\partial C}{\partial t} = D\frac{\partial^2 C}{\partial x^2} \tag{4.2}$$

where C is the concentration of diffusing substance, t is the time, D is the diffusion coefficient inside the studied geometry and x is a characteristic length. The solution to Equation 4.2 is a time-dependent concentration, although to more easily compare different samples it is more convenient to express the release as the fractional release, denoted by $m(t)/m_{\text{tot}}$.

Microcapsules

The solution to the diffusion equation (Equation 4.2) for a monolithic spherical particle is given by Crank [106]. This solution gives an expression for the fractional release (f_s) of an active

substance from monodisperse and monolithic microcapsules of radius r,

$$f_{\mathrm{s}}(D,r,t) = \frac{\alpha_{\mathrm{s}}}{1+\alpha_{\mathrm{s}}}\left[1 - \sum_{n=1}^{\infty} \frac{6\alpha_{\mathrm{s}}(\alpha_{\mathrm{s}}+1)}{9+9\alpha_{\mathrm{s}}+q_{\mathrm{s},n}^2\alpha_{\mathrm{s}}^2} \exp\left(-\frac{Dq_{\mathrm{s},n}^2 t}{r^2}\right)\right]. \tag{4.3}$$

Here, α_{s} is expressed as

$$\alpha_{\mathrm{s}} = \frac{V_{\mathrm{medium}}}{V_{\mathrm{sphere}} K} \tag{4.4}$$

with K as the partition coefficient of the diffusing substance between the microcapsule and the surrounding release medium. V_{medium} and V_{sphere} are the volumes of release medium and microspheres, respectively. The coefficient $q_{\mathrm{s},n}$ is defined as the n:th non-zero positive root of

$$\tan q_{\mathrm{s},n} = \frac{3q_{\mathrm{s},n}}{3+\alpha_{\mathrm{s}}q_{\mathrm{s},n}^2}. \tag{4.5}$$

For the model to be valid, the actives should be molecularly and homogeneously dispersed within the entire microcapsule. Additionally, it is assumed that the volume occupied by the active inside the microcapsule matrix is negligible. The formulated microcapsules are polydisperse, following a size distribution $p(r)$. To account for this polydispersity, the fractional release must be weighted and normalized according to

$$f_{\mathrm{s,\,pd}} = \frac{m(D,t)}{m_{\mathrm{tot}}} = \frac{\int_0^\infty f_{\mathrm{s}}(D,r,t)p(r)r^3\,\mathrm{d}r}{\int_0^\infty p(r)r^3\,\mathrm{d}r}. \tag{4.6}$$

The size distribution $p(r)$ of formulated microcapsules normally follows a log-normal distribution function [107],

$$p(r) = \frac{1}{r\sigma\sqrt{2\pi}} \exp\left(-\frac{(\ln x - \mu)^2}{2\sigma^2}\right), \tag{4.7}$$

where μ and σ are the mean and standard deviation of the logarithmized radius.

In addition to the diffusive release, a burst release [93, 108] is often observed, where a fraction p_{b} of the total release makes up the burst. Assuming this release to follow zero-order kinetics (due to lack of experimental data) during a short time t_{b}, this can be described as

$$f_{\mathrm{s,b}}(t) = \begin{cases} \left(\dfrac{\alpha_{\mathrm{s}}}{1+\alpha_{\mathrm{s}}} - \dfrac{f_0}{p_{\mathrm{b}}}\right)\dfrac{t}{t_{\mathrm{b}}} + \dfrac{f_0}{p_{\mathrm{b}}} & \text{if } t < t_{\mathrm{b}} \\ \dfrac{\alpha_{\mathrm{s}}}{1+\alpha_{\mathrm{s}}} & \text{if } t \geq t_{\mathrm{b}}. \end{cases} \tag{4.8}$$

Here, f_0 is a free non-encapsulated fraction present in the aqueous phase at equilibrium after formulation.

In the case of degradable microcapsules, the final contribution to the observed overall release rate is degradation-controlled release. For the PLGA microcapsules studied in Paper IV and Paper VII, this was the rate-limiting release event at long times.

For a given PLGA polymer segment P with a degree of polymerization of n, its acid-catalyzed hydrolysis into two smaller segments of length m and n-m can be described [109] as

$$\mathrm{P}_i + \mathrm{H_2O} + \mathrm{H^+} \rightarrow \mathrm{P}_m + \mathrm{P}_{n-m} + \mathrm{H^+}, \quad n = 2,3,..., \text{ and } m = 1,2,...,n-1$$

Both P_m and P_{n-m} will contain one acid and one alcohol end group, leading to a net generation of acid groups that induces an autocatalytic degradation of the polymer. The acid-catalyzed degradation of a polyester can therefore be described with a rate expression [110] describing the change in concentration of carboxylic acid groups,

$$\frac{\mathrm{d[A]}}{\mathrm{d}t} = k_\mathrm{d}[\mathrm{A}][\mathrm{E}][\mathrm{H_2O}]. \tag{4.9}$$

Here, [A] and [E] are the concentrations of acid and ester groups, respectively, and k_d is a rate constant for the reaction. Since the diffusion of water into the microcapsules generally is faster than the degradation reaction [94], water is normally assumed to be in excess which leads to a modified second-order rate expression [111] of the form

$$\frac{\mathrm{d[A]}}{\mathrm{d}t} = k_\mathrm{d2}[\mathrm{A}][\mathrm{E}] = k_\mathrm{d2}([\mathrm{A}]_0 + [\mathrm{A}])([\mathrm{E}]_0 - [\mathrm{A}]) \tag{4.10}$$

with a rate constant k_d2 and the solution

$$[\mathrm{A}](t) = [\mathrm{A}]_0 \frac{\exp(c_1 t) - 1}{1 + c_2 \exp(c_1 t)} \tag{4.11}$$

where the subscript 0 denotes the initial concentration at time zero, and the coefficients c_1 and c_2 are defined as

$$c_1 = ([\mathrm{A}]_0 + [\mathrm{E}]_0) k_\mathrm{d2} \tag{4.12}$$

$$c_2 = \frac{[\mathrm{A}]_0}{[\mathrm{E}]_0} \tag{4.13}$$

Assuming that the number of formed acid groups is proportional to the release of actives, Equation 4.11 must be normalized and rescaled to yield the fractional release of active by degradation as

$$f_\mathrm{d2}(t) = \frac{\alpha_\mathrm{s}}{1+\alpha_\mathrm{s}} + \left(1 - \frac{\alpha_\mathrm{s}}{1+\alpha_\mathrm{s}}\right) \frac{[\mathrm{A}](t)}{[\mathrm{E}]_0 + [\mathrm{A}]_0}. \tag{4.14}$$

If the release medium contains solubilizing agents, such as the Brij L23 used here, yet another simplification can be done to the rate expression in Equation 4.9. Formed PLGA oligomers

bearing carboxylate groups will be released and solubilized in the aqueous phase, thus leading to an approximately constant and low acid concentration. In this case, the rate expression can be further reduced to a pseudo-first order expression with the fractional release as

$$f_{\mathrm{d1}}(t) = \left(1 - \frac{\alpha_{\mathrm{s}}}{1+\alpha_{\mathrm{s}}}\right)(1 - \exp(-k_{\mathrm{d1}}t)) \tag{4.15}$$

where k_{d1} is an apparent pseudo-first order rate constant.

Combining the burst and diffusion-controlled release with the degradation-controlled release, the final expression for the observed fractional release $f_{\mathrm{s,\,release}}$ is given by

$$f_{\mathrm{s,\,release}} = f_0 + p_{\mathrm{b}} f_{\mathrm{s,b}}(t) + (1-p_{\mathrm{b}}) f_{\mathrm{s,pd}}(D,t) + f_{\mathrm{d}i}(t). \tag{4.16}$$

Analytical solutions to the diffusion-controlled release have been proposed for core-shell microcapsules as well [112], although the analytical solution to such a problem is significantly more complex as compared to monolithic microcapsules.

Fibrous materials

Similar to release from microcapsules, the diffusion in fibers can also be modeled. The fractional release from a fiber (f_{c}) in which the diffusing substance initially is homogeneously distributed can be modeled by a cylindrical geometry. This is described by Crank [106],

$$f_{\mathrm{c}}(r,t) = \frac{\alpha_{\mathrm{c}}}{1+\alpha_{\mathrm{c}}}\left[1 - \sum_{n=1}^{\infty} \frac{4\alpha_{\mathrm{c}}(\alpha_{\mathrm{c}}+1)}{4+4\alpha_{\mathrm{c}}+q_{\mathrm{c},n}^2\alpha_{\mathrm{c}}^2} \exp\left(-\frac{Dq_{\mathrm{c},n}^2 t}{a^2}\right)\right], \tag{4.17}$$

where a is the radius of the fiber. The parameter α_{c} is defined as

$$\alpha_{\mathrm{c}} = \frac{V_{\mathrm{medium}}}{V_{\mathrm{cyl}}K} \tag{4.18}$$

with V_{cyl} being the volume of the cylinder. For a cylinder, $q_{\mathrm{c},n}$ is defined as the n:th non-zero positive root of

$$\alpha_{\mathrm{c}} q_{\mathrm{c},n} J_0(q_{\mathrm{c},n}) + 2J_1(q_{\mathrm{c},n}) = 0. \tag{4.19}$$

Here, J_0 and J_1 are the Bessel functions of the first kind of order 0 and 1, respectively,

$$J_m(x) = \sum_{k=0}^{\infty} \frac{(-1)^k}{k!\Gamma(k+m+1)}\left(\frac{x}{2}\right)^{2k+m} \tag{4.20}$$

where $\Gamma(z)$ is the Gamma function,

$$\Gamma(z) = \int_0^{\infty} t^{z-1}e^{-t}\mathrm{d}t. \tag{4.21}$$

Similar to the microcapsules, polydispersity in the fiber radii is taken into account by weighting and normalizing the fractional release,

$$f_{\text{c, pd}} = \frac{m(t)}{m_{\text{tot}}} = \frac{\int f_{\text{c}}(a,t)p(a)a^2 \, \mathrm{d}a}{\int p(a)a^2 \, \mathrm{d}a}. \tag{4.22}$$

Burst contributions may be included in the expression for the fractional release like in Equations 4.8 and 4.16 as

$$f_{\text{c,b}}(t) = \begin{cases} \left(\dfrac{\alpha_{\text{c}}}{1+\alpha_{\text{c}}} - \dfrac{f_0}{p_{\text{b}}} \right) \dfrac{t}{t_{\text{b}}} + \dfrac{f_0}{p_{\text{b}}} & \text{if } t < t_{\text{b}} \\ \dfrac{\alpha_{\text{c}}}{1+\alpha_{\text{c}}} & \text{if } t \geq t_{\text{b}} \end{cases} \tag{4.23}$$

$$f_{\text{c, release}} = p_{\text{b}} f_{\text{c,b}}(t) + (1-p_{\text{b}}) f_{\text{c,pd}}(D,t). \tag{4.24}$$

When the active substance is impregnated onto the fiber surface, rather than homogeneously distributed in the fiber bulk, part of the active may still permeate into the fiber from where it will be slowly released following a diffusive process. Parts of the active will in that case be deposited on the fiber surface from where it will be rapidly released, similar to the burst release described in Equation 4.23. The slower, diffusional contribution to the release $f_{\text{p}}(D,L,t)$ can be approximated as diffusion from a plane sheet [106],

$$f_{\text{p}}(D,L,t) = 1 - \sum_{n=0}^{\infty} \frac{8}{(2n+1)^2\pi^2} \exp\left(- \frac{D(2n+1)^2\pi^2 t}{4L^2} \right), \tag{4.25}$$

where L is the thickness of the sheet. Combined, the final expression for the fractional release from the surface impregnated material is

$$f_{\text{p, release}} = p_{\text{b}} f_{\text{c,b}}(t) + (1-p_{\text{b}}) f_{\text{p}}(D,L,t). \tag{4.26}$$

5

Microencapsulation Enables Rate-limiting Release

5.1 A Unified Theory for Microcapsule Morphology Prediction

The morphology of formulated microcapsules is decisive for their function. Consequently, accurate theories for morphology prediction are vital in microcapsule development. The thermodynamical theory based on spreading coefficients in Equations 3.2-3.5 can be a powerful tool in morphology prediction. When applied to microcapsules based on both poly(methyl methacrylate) (PMMA) and poly(D,L-lactic-*co*-glycolic acid) (PLGA) shells containing a hexadecane core, core-shell morphologies are successfully predicted for both systems. Figure 5.1a4 and Figure 5.1b4 do, however, demonstrate significant differences in the observed morphologies for these two microcapsule systems. Although core-shell morphologies are observed in both cases, the thermodynamical approach in Equations 3.2-3.5 – considering only the final state of the microcapsule – does not describe the highly offset core in the PLGA-based microcapsules. Such morphological weak spots can be utilized to achieve an instantaneous stimuli-responsive release as demonstrated in Paper II. If on the other hand applications for sustained release are envisaged, it is beneficial to formulate microcapsules containing a centrally placed core. To improve the accuracy of morphology prediction and explain this morphological difference in core positioning, an expanded theory that additionally considers the entire formation pathway was introduced in Paper I.

The process of internal phase separation by solvent evaporation is by definition a non-equilibrium process. As the volatile solvent evaporates, it continuously alters the phase compositions, consequently affecting the interfacial tensions that dictate the thermodynamic spreading coefficients of the system. It was therefore hypothesized that any formed intermediate morphologies play a central role in deciding the morphological outcome of the formulation. The evolution of intermediate morphologies was therefore determined for microcapsules based on both PMMA and PLGA shells with molecular weights of 25 and 10 kDa, respectively, as shown in Figure 5.1a-b. Initially, an emulsion was formed where all

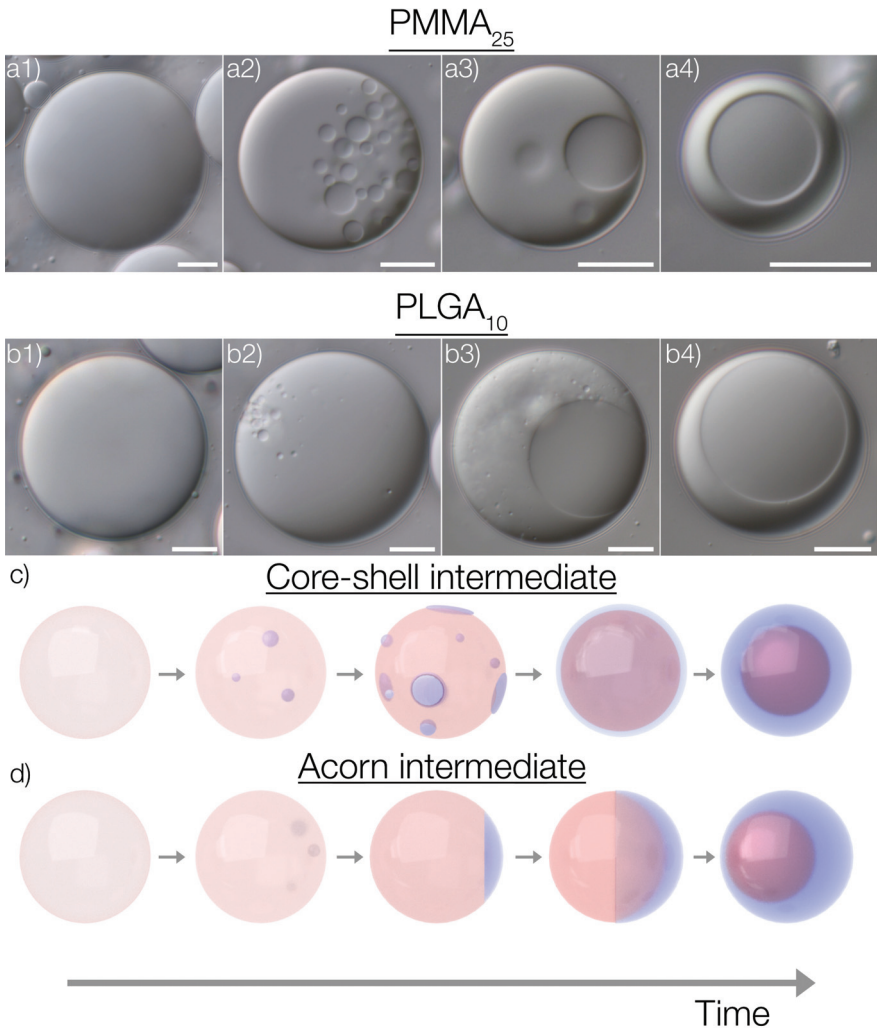

Figure 5.1: Microscopic snapshots of internal phase separation in emulsion droplets acquired during evaporation of DCM for a) $PMMA_{25}$ and b) $PLGA_{10}$ microcapsules. Micrographs in 1) were taken immediately after emulsification, and 2-3) were taken successively shortly after entering the two-phase region. The micrographs in a4) and b4) show the obtained final morphologies after evaporating all volatile solvent overnight. Scale bars are 5 µm. In c) and d), illustrations of formation pathways for intermediate core-shell and acorn morphologies, respectively, are shown.

the microcapsule components were dissolved. At some point following solvent evaporation, coacervation begins as the emulsion droplet enters a two-phase region. The morphology of this initial intermediate morphology is controlled solely by the interfacial tensions between these intermediate phases and by extension its intermediate spreading coefficients. Intermediate acorn morphologies were observed for both PMMA and PLGA microcapsules as shown in Figure 5.1a-b. Consequently, during the internal phase separation of both systems, there was a transition point from the intermediate acorn morphology to the final core-shell structure. Once the core-shell morphology forms – whether the core is centered or offset – there is no thermodynamical advantage of further centering the core. Therefore, the extent of

core offset and minimum shell thickness will be controlled by the point in the emulsion droplet phase diagram at which the transition from acorn to core-shell occurs. An earlier transition gives a larger amount of shell growth in the core-shell region, and consequently a more centered core. This is visualized schematically in Figure 5.1c-d for two examples of intermediate core-shell and acorn morphologies, respectively. Applying this concept to the observed morphologies of the PMMA- and PLGA-based microcapsules, the transition to the final core-shell region for the PMMA microcapsules was hypothesized to have occurred when a larger fraction of volatile solvent remained.

5.1.1 Intermediate Spreading Coefficients

To test this hypothesis, interfacial tensions, and by extension spreading coefficients, were measured over the course of the entire evaporation event. The full evolution of the spreading coefficients, expressed based on both the volatile solvent mass fraction remaining and time, is shown in Figure 5.2. For both of the studied systems, $S_p < 0$ was initially true, indicating a preference for an intermediate acorn-like morphology as evidenced by the micrographs in Figure 5.1. Upon analyzing the evolution of S_p for these systems, a key difference was

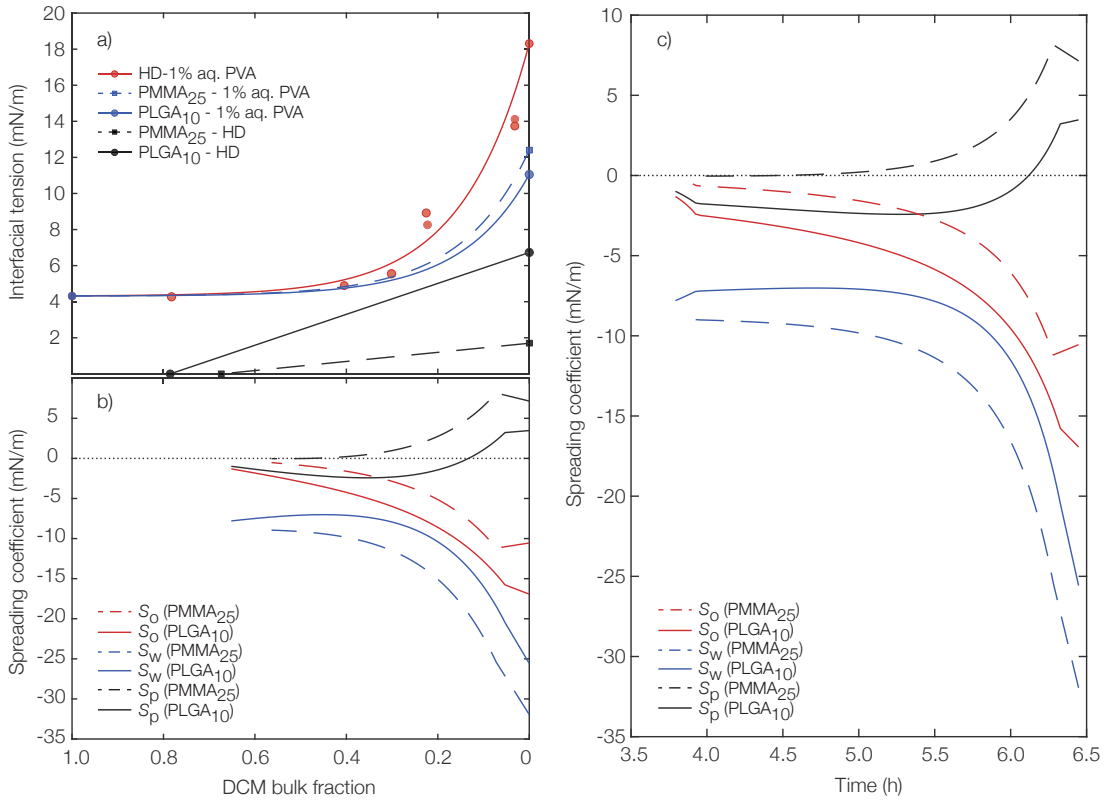

Figure 5.2: a) Interfacial tensions for the ternary microcapsule systems with $PMMA_{25}$ and $PLGA_{10}$ shells. In b) and c) calculated intermediate spreading coefficients are expressed based on DCM mass fraction and time, respectively.

observed. For the PMMA-based system, S_p rapidly became increasingly positive which meant that a core-shell intermediate was the preferred morphology over the majority of the two-phase region. On the contrary, for the PLGA microcapsules $S_p < 0$ was true over a large portion of the formation event with an intermediate acorn as the preferred morphology. It was only in the final 20 minutes of the evaporation event that a core-shell morphology was predicted for the PLGA microcapsules. Thus, only a small fraction of the PLGA was available to form a uniform shell around the microcapsule, resulting in a highly offset core.

The origin of the morphology difference was consequently verified to be the point at which the transition from an intermediate acorn to core-shell morphology occurred. The driving factor for this difference was the polymer-oil interfacial energy. PMMA exhibited a considerably lower γ_{po} over the entire formation process, implying that the formation of a large interface between these phases, i.e., the core-shell morphology, gave a smaller energy penalty as compared to its PLGA counterpart. Additionally, despite the more hydrophobic nature of PMMA, its interfacial tension against the aqueous phase remained nearly identical to PLGA. This was likely due to the PVA acting as the main factor in controlling the interfacial energy in both cases, which further affected the difference in morphology.

5.1.2 The Microcapsule Formation Pathway

Analyzing the evolution of the *spreading plot* in Figure 5.2 requires knowledge of the phase behavior of the two-phase emulsion droplets. Two pedagogical and schematic examples of phase diagrams with corresponding morphology predictions are shown in Figure 5.3. Any microcapsule formulation following internal phase separation follows a certain *formation pathway* through the phase diagram, defined by the shell-to-core (m_s/m_c) ratio. At the point of entering the two-phase region of the phase diagram, all possible morphologies can form – whether inverted core-shell, acorn, or core-shell. This initial intermediate morphology is solely controlled by thermodynamics. From this point, the progression is influenced by the shape of the two-phase region as well as the slope of its tie-lines. For producing perfectly centered core-shell microcapsules, the only predicted intermediate morphology should be core-shell. This morphology can be promoted by maintaining a high interfacial tension between the emulsion droplet and aqueous phase, while at the same time minimizing the polymer-water interfacial tension. By employing for example anchoring block co-polymer dispersants [113, 114] in the aqueous phase this can be achieved.

For systems presenting inconstant intermediate morphologies, kinetic parameters become increasingly important. The rate of formation is governed by the rate of solvent evaporation from the emulsion, influenced by factors such as temperature, ambient pressure, vapor pressure, and aqueous saturation concentration of the organic volatile solvent. A rapid formation process can kinetically trap intermediate morphologies if sufficient equilibration time is not given. In Paper I trapped intermediate acorn particles were formulated, trapped

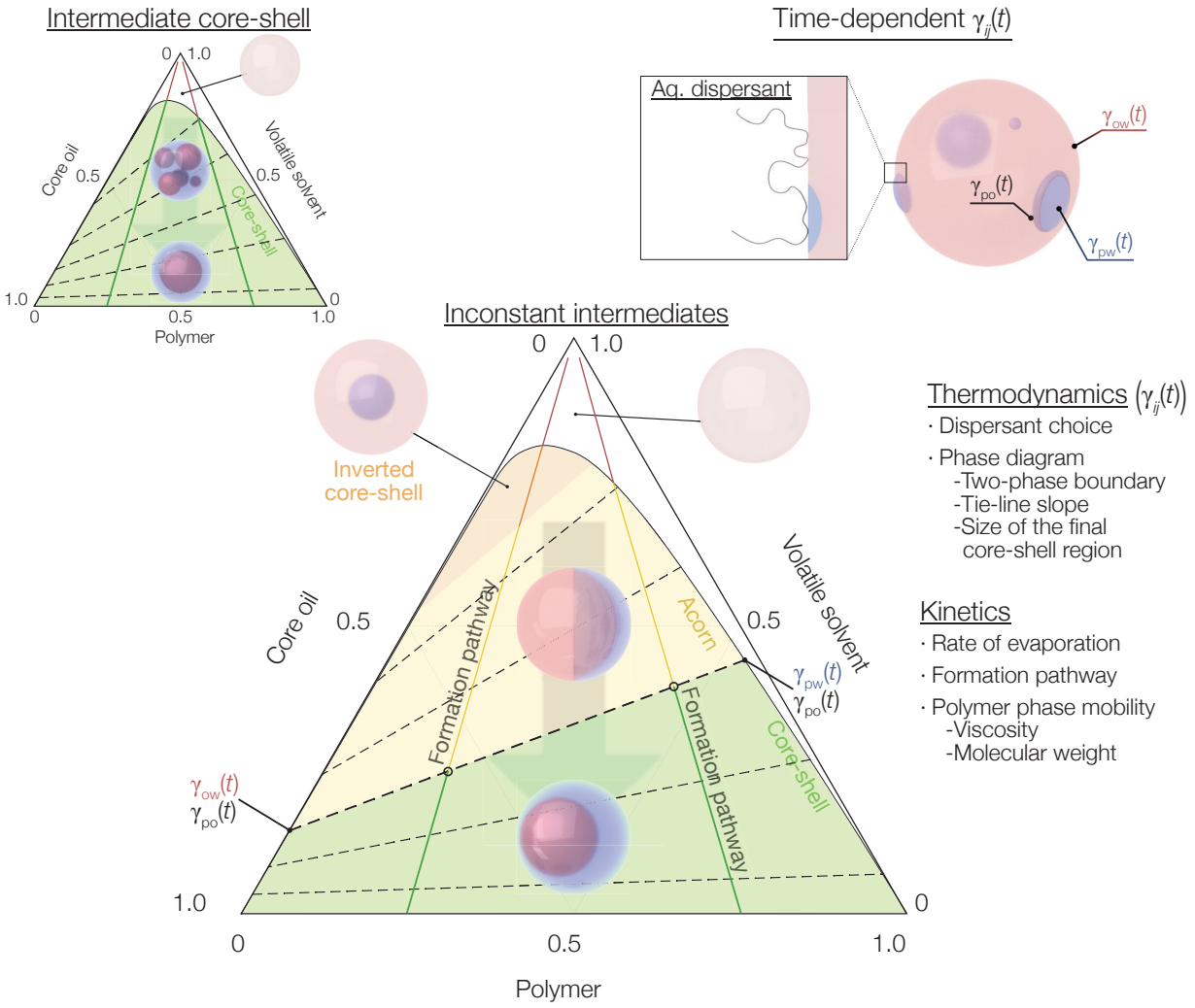

Figure 5.3: Illustrative phase diagrams showing the formation of intermediate core-shell and intermediate inverted core-shell and acorn microcapsules with their respective end products after equilibration. Regions in the phase diagram with a thermodynamically favored intermediate core-shell is shaded in orange, acorn in yellow, and core-shell regions in green. Two formation pathways for different m_s/m_c-ratios are shown in each phase diagram. The relevant time-dependent interfacial tensions are highlighted, and the key thermodynamic and kinetic factors controlling the microcapsule morphology are summarized.

multicore microcapsules were found in both Paper I and Paper II, and in Paper III intermediate inverted core-shell microcapsules were formulated. This highlights the broad range of possible kinetically trapped intermediate morphologies, all of which could be explained by considering the entire formation pathway.

Yet another aspect affecting the impact of kinetic considerations is the molecular weight of the shell polymer. An increased molecular weight leads to an increasing viscosity of the polymer-rich phase, which in turn leads to slower equilibration. To summarize, it becomes evident that both the size of the final core-shell area in the phase diagram (controlled by thermodynamics) as

well as the time spent in this region (controlled by formation kinetics) are crucial for controlling the microcapsule morphology. Moreover, in a two-phase region with pronounced tie-line slopes, the m_s/m_c-ratio also influences the size of the morphology domains. As depicted for the system of inconstant intermediates in Figure 5.3, the two formation pathways demonstrate that a higher m_s/m_c ratio (evolving through the rightmost part of the phase diagram) would allow for more time in the final core-shell region.

5.2 Stimuli-responsive Release

An instantaneous and on-demand release can be achieved by formulating microcapsules with shells that are sensitive to external stimuli. Depending on the application, a range of different stimuli can be utilized. This work has studied the feasibility of two different triggering mechanisms: pH changes in Paper II, and UV light exposure in Paper III. These microcapsules and the components used in their formulation are depicted schematically in Figure 5.4. In both cases, the model active substance pyrene was encapsulated and molecularly dissolved in the core oil.

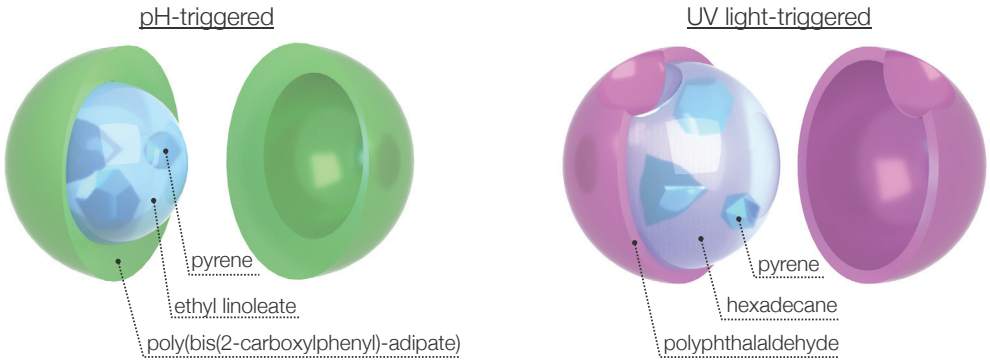

Figure 5.4: Schematic illustration of the components used in the formulation of stimuli-responsive microcapsules sensitive to pH-changes and UV light, respectively.

5.2.1 pH-triggered Release

Polyanhydride core-shell microcapsules encapsulating the model active substance pyrene dissolved in ethyl linoleate were formulated in Paper II. As shown in the insets of Figure 5.5, microcapsules displaying both single core and multicore morphologies were formulated by varying the shell-to-core ratio (m_s/m_c) to evaluate the effect of internal microcapsule morphology. This difference in morphology was controlled by kinetically trapping an intermediate multicore morphology as discussed in Section 5.1 and in Paper I. In acidic pH, neither morphology exhibited triggered release. Instead, a slow and sustained release occurred, controlled by the diffusive barrier of the shell. The burst release observed in these cases originated from the rapid solubilization of pyrene dissolved in oil droplets not

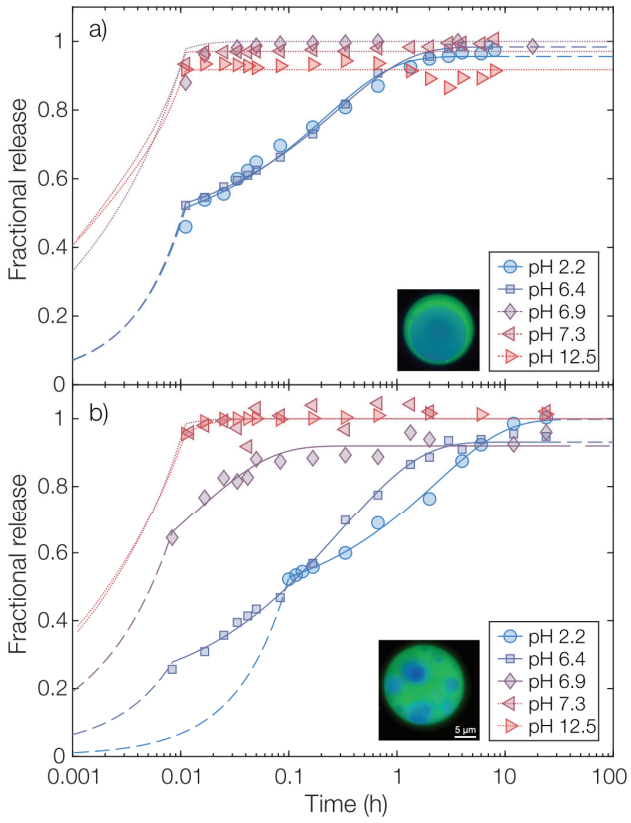

Figure 5.5: Fractional release from microcapsules with an m_s/m_c-ratio of a) 2.5 and b) 5.0, evaluated in release media with pH values ranging from 2.2 to 12.5. Experimental data points are shown along with fitted diffusion models in dashed and solid lines. Dotted lines are modeled threshold values for the apparent diffusivity given the temporal resolution of the experiments and are consequently only lower limits.

successfully encapsulated during formulation. This encapsulation efficiency was improved by increasing the m_s/m_c-ratio.

By increasing the pH of the continuous phase, the remarkable pH sensitivity of the polyanhydride was demonstrated. Changing the pH from 6.4 to 6.9 entirely shifted the release behavior from diffusion-controlled to degradation-controlled, resulting in a complete release within less than one minute of exposure. It should be emphasized that this was a significantly faster degradation of the polymer shell than the slow erosion of polymers like the PLGA discussed in Section 5.3. From the multicore microcapsules in Figure 5.5b, a slightly less responsive release was observed. While difficult to determine experimentally, the average shell thickness in this system was likely greater than in the single core microcapsules in Figure 5.5a. As a consequence, a more extensive polymeric shell degradation was required before releasing the entire core content.

The release data were described by a diffusion model (Equation 4.6) for quantification of the release rates through apparent pyrene diffusion coefficients, represented by the lines in Figure 5.5. It must be emphasized that this is not the true diffusion coefficient in the microcapsule shell, but rather an apparent diffusion coefficient across all microcapsule compartments. The concept of apparent diffusion coefficients is discussed in more detail in connection to the microcapsule-functionalized fibrous materials in Chapter 6. For diffusion control at low pH values, the data was well-fitted by this model with apparent diffusion coefficients presented in Figure 5.6a. In the degradation-controlled regime at higher pH, the release rate exceeded the resolution of the experimental sampling method, making precise measurement challenging. Therefore, Figure 5.6a only displays the detection limits for these measurements. However, it was evident that the apparent diffusivity increased by at least two orders of magnitude across this narrow pH range.

In addition to measuring the release of the encapsulated active, the degradation kinetics of the polymeric shell itself was determined. The presence of the salicylic acid group in the polymer backbone (see Figure 3.3c) facilitated the quantification of the extent of depolymerization

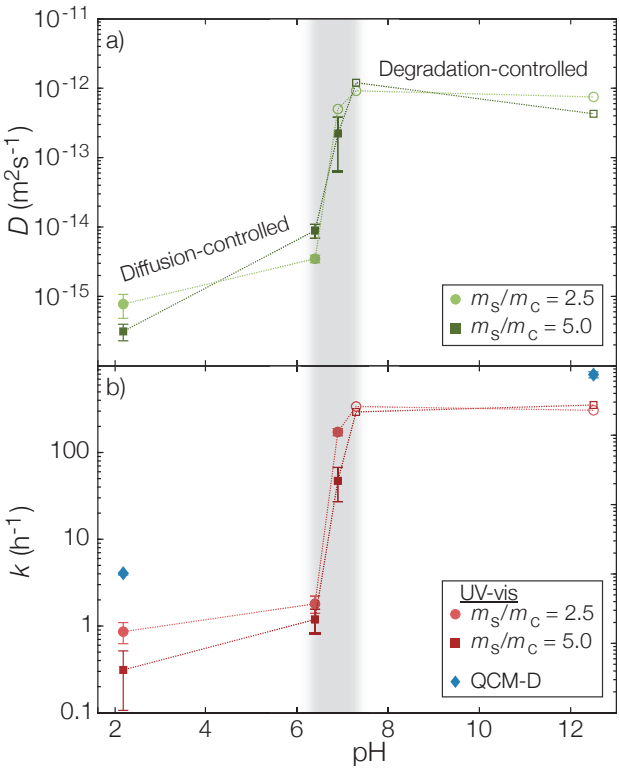

Figure 5.6: a) Fitted diffusion coefficients (±95% confidence interval of fit) from microcapsules with an m_s/m_c-ratio of 2.5 and 5.0. b) Fitted rate constants for the polyanhydride degradation based on spectrophotometry and QCM-D. All open markers in both subfigures are modeled threshold values given the temporal resolution of the experiments, and consequently only lower limits.

using UV-vis spectrophotometry. Similar to the release of pyrene over time, the increasing concentration of solubilized monomeric or oligomeric degradation products in the aqueous phase was measured. This degradation by hydrolysis was assumed to occur with an excess of water, leading to a pseudo-first order rate expression for the degradation, Equation 4.15. This model was found to describe the experimental data well, leading to the fitted apparent rate constants in Figure 5.6b. Here a strong correlation could be observed between the apparent diffusivity and degradation rate constant with a 100-fold increase in both quantities over the narrow pH interval of 6.4 to 6.9.

To gain a mechanistic understanding of the release and the processes involved in the triggering event, in-situ microscopy of the microcapsules during exposure to a release medium at pH 7.3 was performed. Within less than one minute of exposure, small pores began forming across the entire microcapsule surface, as illustrated in Figure 5.7b. As exposure continued, large-scale cracks emerged that fully exposed the core oil phase. The polymeric shell transitioned to become increasingly liquid-like as the degradation progressed further, clearly depicted in the altered morphology after 20 minutes of exposure in Figure 5.7e.

As discussed earlier, the single-core microcapsules exhibited an offset core morphology with uneven shell thickness. It could be observed that the microcapsules ruptured in the area where the shell was the thinnest, indicating that this served as a designed morphological weak spot. This morphological weak spot present in only the single-core microcapsules could also describe the slight discrepancy in release behavior at the onset of degradation-controlled release (pH 6.9).

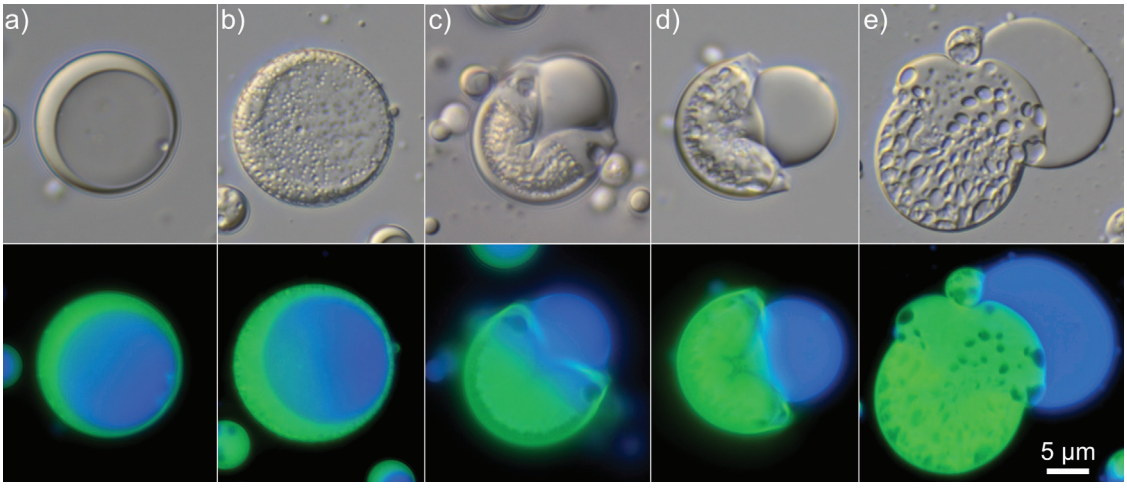

Figure 5.7: Morphological evolution over time as microcapsules ($m_s/m_c = 2.5$) were exposed to an aqueous phase of pH 7.3. The appearance in c) was seen within minutes of exposure, whereas e) was after 20 minutes. Polyanhydride autofluorescence can be seen (green) and differentiated from pyrene dissolved in the ethyl linoleate core oil (blue). The scale bar is valid for all subfigures.

The in situ degradation study clearly highlights one of the main benefits of utilizing core-shell microcapsules for a triggered release of actives, as compared to monolithic microspheres. A small fraction of shell degradation is sufficient to form pores or cracks in the microcapsule shell, from which all of the active can be released instantaneously. Therefore, the pores formed already in Figure 5.7b may have provided sufficient permeability to enable an instantaneous release. In the case of a monolithic microsphere, the entire particle must degrade in order to release all of the encapsulated active substance. As evident from the studies on the polymer degradation kinetics, this is a significantly slower process that prevents an instantaneous release.

5.2.2 UV Light-triggered Release

Similar to the morphological weak spot in the polyanhydride microcapsules in Paper II, a morphological weak spot was desired for the polyphthalaldehyde (PPA) microcapsules formulated in Paper III. Two polymeric dispersants were investigated for their effects on the formulation: poly(vinyl alcohol) (PVA) and poly(methacrylic acid) (PMAA). The obtained microcapsule morphologies from stabilization by these two dispersants are shown in Figure 5.8. A mixture of core-shell and acorn microparticles could be observed in the PVA-stabilized system, whereas a blueberry morphology was obtained when stabilizing with PMAA. To further understand these morphologies, the spreading coefficients for each system were calculated as presented in Table 5.1. In both cases the spreading coefficient S_p was close to zero, indicating a boundary state between core-shell and acorn morphologies. The notably high interfacial tension between PPA and pure water indicated a highly hydrophobic nature of

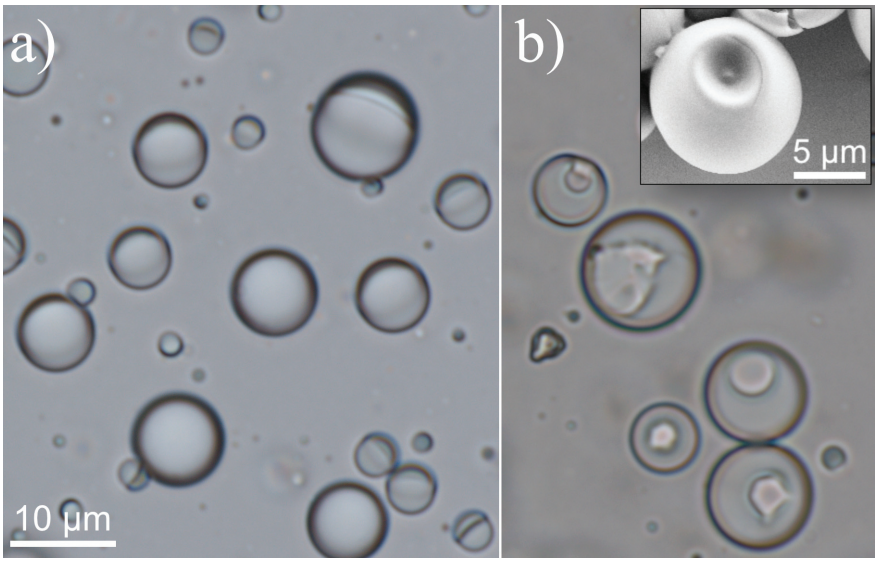

Figure 5.8: Optical micrographs of the microcapsule morphologies obtained when stabilizing with a) PVA and b) PMAA. The inset shows a SEM micrograph of a dried PMAA blueberry microcapsule. The scale bar is valid for both sub-figures.

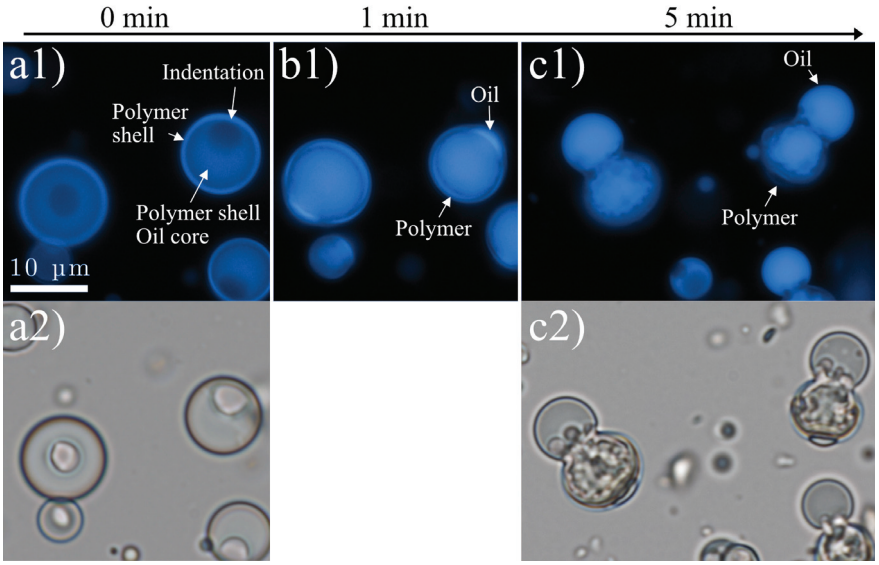

Figure 5.9: In situ-triggered release from PMAA-stabilized microcapsules in water suspension after a) 0 min., b) 1 min., c) 5 min. as shown by both fluorescence and brightfield micrographs. The scale bar is valid for all sub-figures.

the polymer. The effectiveness of the dispersant in significantly reducing this polymer-water interfacial tension was the driving factor for core-shell particle formation over acorn microparticles. This is an uncommon occurrence, as it is typically the dispersant's ability to maintain a large oil-water interfacial tension that promotes core-shell formation.

The triggered release from PPA-microcapsules was investigated from microcapsules in an aqueous suspension and is shown for PMAA-stabilized microcapsules in Figure 5.9. After one minute of UV light exposure, the oil core was seen to begin protruding from the cavity in the blueberry microcapsules. After five minutes, the entire oil phase had emerged from the microcapsules. In all capsules, the oil was protruding from the blueberry cavity. It was therefore hypothesized that this was the weakest part of the microcapsule. In terms of triggered release, this designed weakness was highly beneficial since it allowed for a fast and almost

Table 5.1: Interfacial tensions and calculated spreading coefficients for the different dispersants, along with predicted and observed microcapsule morphologies. All values are in mN/m.

Dispersant	γ_{ow}	γ_{op}	γ_{pw}	S_p	S_w	S_o	Morphology	
							Predicted	Observed
None	53.5	14.4	43.3	-4.2	-82.3	-24.7	Acorn	-
PVA	21.2	14.4	4.2	2.6	-11.0	-31.5	Core-shell	Acorn Core-shell
PMAA	33.4	14.4	19.4	-0.4	-38.4	-28.5	Acorn	Blueberry

instantaneous release of the core contents. Without a blueberry cavity, as was the case for PVA-stabilized microcapsules, no protruding core oil was seen even with longer exposure times. There was, however, a visible deformation of the shell but not to the point where the capsule wall collapsed to release the core oil.

5.3 Sustained Release

In Paper IV, a formulation aimed at achieving sustained release of the active antimicrobial agent octenidine dihydrochloride (OCT) was developed. OCT differed from the model active pyrene in two significant aspects: its cationic charge and notable aqueous solubility. These differences allowed for the implementation of strategies beyond purely hydrophobic interactions to enhance encapsulation and release properties. Encapsulation was carried out in monolithic PLGA microspheres where OCT was molecularly dispersed in the microcapsule matrix, illustrated schematically in Figure 5.10. Prior hypotheses have suggested that OCT was encapsulated in similar lactide-based polymers through electrostatic interactions between the cationic OCT and anionic carboxylate end groups in the polymer [115]. In Paper IV, this electrostatic interaction was confirmed through infrared spectroscopy. The maximum loading capacity in the microcapsules was 51 µmol OCT/g PLGA (equivalent to 3.2 wt.%). Comparing this to the total amount of acid groups in the polymer (168 µmol/g) and assuming both cationic sites on OCT bind, about two-thirds of the available sorption sites were utilized for binding OCT. This further strengthened the evidence for a strong binding of OCT to the microcapsule matrix.

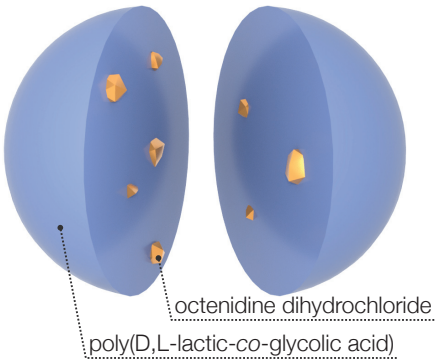

Figure 5.10: Schematic illustration of a sustained release monolithic PLGA microcapsule.

The release of OCT from the microcapsules was studied in an aqueous TRIS-buffered release medium at pH 7.4 containing 0.5 wt.% Brij L23 ($C_{12}E_{23}$) nonionic surfactant at both ambient (22 °C) and physiological (37 °C) temperatures as shown in Figure 5.11. The microcapsules were loaded with 5 wt.% OCT during formulation, to reach the maximum loading capacity of 3.2 wt%. Consequently, the remaining OCT was present in the aqueous phase in the formulated suspension and at the initial point of the release measurement ($f_0 = 0.34$). Starting at f_0, three distinct contributions to the release profiles were identified: (*i*) burst release, (*ii*) diffusion-controlled release, and (*iii*) degradation-controlled release. A burst release of around 20% was observed at both temperatures and was most likely a result of releasing OCT bound to the surface of the microcapsules.

In the diffusion-controlled regime, an increasing diffusivity was found with increasing temperature. This effect was quantified by fitting the diffusion model in Equation 4.16,

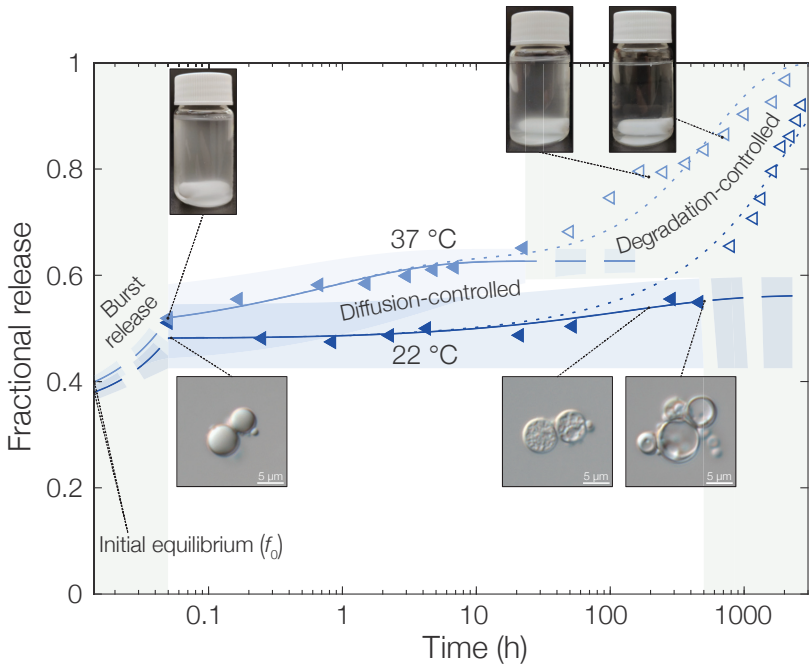

Figure 5.11: Fractional release of OCT from PLGA microcapsules at both 22 °C and 37 °C in TRIS-buffered 0.5% aqueous Brij L23 at pH 7.4. Experimental data points are shown along with fitted diffusion models. Shaded areas correspond to a 95% confidence interval for the fitted parameters. Filled markers indicate the area where the diffusion equation was fitted and valid without PLGA degradation affecting the release rate. In the dotted lines, the degradation rate expression has been included. Photographs and micrographs in the insets display the gradual degradation of the microcapsules over time on both a macroscopic and microscopic scale.

omitting the degradation contribution, to the data in the diffusion-controlled regime. An apparent diffusion coefficient approximately 200 times greater was found at 37 °C compared to 22 °C. An Arrhenius relationship might partially explain this phenomenon of increasing diffusivity, however, it was likely also influenced by surpassing the glass transition temperature of PLGA, approximately 30 °C in its hydrated state [116]. Above the glass transition temperature, the free volume of the polymer increases, leading to an increased mobility of OCT and consequently an increased diffusivity.

Temperature dependence was not only observed in the diffusion-controlled regime but also in the degradation rate of PLGA and the onset of the degradation-controlled regime. At 22 °C, the release followed the diffusion model for the initial two weeks (400 hours), whereas at 37 °C, diffusion-controlled release was only observed during the first day. Beyond this point, degradation became so significant that the release shifted to a regime where bound OCT was released through hydrolysis of the PLGA matrix into water-soluble monomeric or oligomeric fragments. This final degradation was assumed to follow apparent pseudo-first order kinetics with an excess of water (Equation 4.15). Thus, the overall observed release was well-described by Equation 4.16 as shown by the dotted lines in Figure 5.11. The transition to the degradation-

controlled regime was also evident in the changing morphology of the microcapsules, as shown in the insets in Figure 5.11. Over time, water-filled pores formed and expanded until the entire microcapsule disintegrated, as seen by the transition from an opaque to transparent release medium.

The implications of the OCT-binding to PLGA were further quantified by extending the diffusion model to incorporate the binding event. The diffusivity of an active in a matrix is typically a composite quantity influenced by a range of factors beyond the free diffusivity D_0, including macroporosity, microporosity (e.g., free volume), tortuosity, and notably, specific interactions between the active and matrix [48]. The observed diffusivity, considering all these factors, is often referred to as the *effective* diffusion coefficient. When the binding is strong, only the free fraction k_I is available for diffusion, leading to

$$D_\mathrm{eff} = D_0 \left[\exp\left(-\gamma \frac{V_\mathrm{c}}{V_\mathrm{f}} \right) \frac{\varepsilon}{\tau} \right] k_\mathrm{I}. \tag{5.1}$$

All parameters within the brackets describe the effects of porosity and tortuosity and were assumed to remain constant for the PLGA microcapsules at a specific temperature. The release of OCT from loaded microcapsules gave a measure of D_eff using the method described earlier. To measure D_0, plain PLGA microcapsules without any loading were introduced into a release medium already containing dissolved OCT. During this measurement of OCT uptake into the microcapsules, OCT would freely diffuse until encountering an available binding site in the polymer matrix. By measuring both D_eff and D_0 as shown in Figure 5.12, the freely diffusing fraction k_I could be determined.

It was furthermore verified that the release medium and the solubilizing surfactant did not affect the internal properties of the microcapsules by measuring both release and uptake at two different solubilizer concentrations as well as in a reference medium without solubilizer. An equal diffusivity was found in all three media, verifying that any swelling of the microcapsule matrix could be neglected. However, as expected, the presence of a solubilizer affected the partitioning of OCT between the microcapsules and release medium. As shown in Table 5.2, the binding caused a decrease in the effective diffusivity by about one order of magnitude as compared to the free diffusivity, and by extension a k_I of around 0.1 was found at both ambient and physiological temperatures.

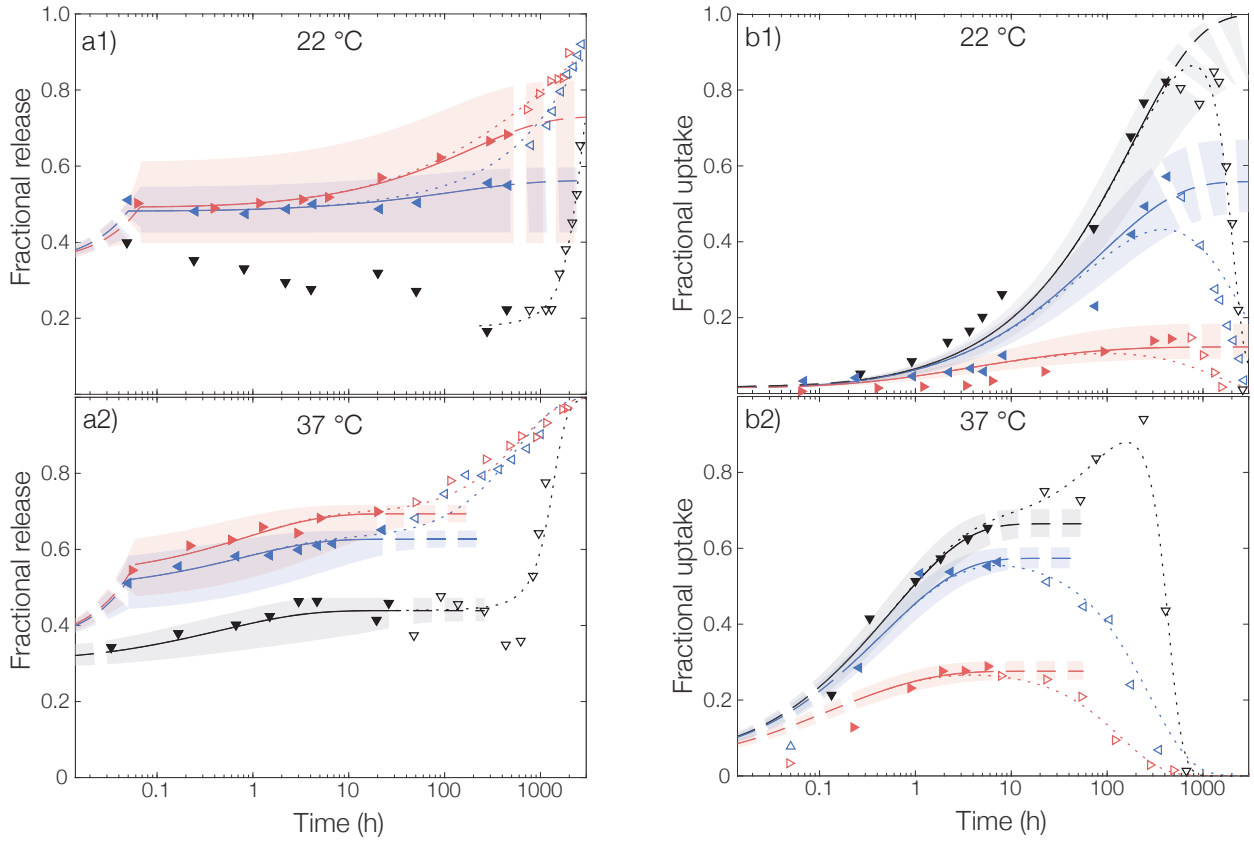

Figure 5.12: a) Release of OCT from PLGA microcapsules and b) corresponding uptake of OCT, measured in TRIS-buffered release media at pH 7.4 with 0% (▼), 0.5% (◀), and 6% (▶) Brij L23. Measurements were performed at 1) 22 °C and 2) 37 °C, respectively. Experimental data is shown along with globally fitted diffusion models, fitted only to the filled data points. Shaded areas correspond to a 95% confidence interval for the fitted parameters. The model shown with a dotted line additionally includes release caused by polymer degradation.

Table 5.2: Fitted diffusion coefficients and release burst fractions for release and sorption studies in release media with different concentrations of solubilizing Brij L23 at 22 °C and 37 °C along with k_I calculated from fitted $D_{sorption}$ and $D_{release}$. Values are presented with a 95% confidence interval for the fitted parameters.

22 °C			
Brij L23 fraction (wt.%)	D_{eff} $\left(m^2 s^{-1}\right)$	D_0 $\left(m^2 s^{-1}\right)$	k_I
0	-	$(4.1 \pm 1.7) \cdot 10^{-19}$	-
0.5	$(5.0 \pm 6.0) \cdot 10^{-20}$		0.12 ± 0.16
6.0			

37 °C			
Brij L23 fraction (wt.%)	D_{eff} $\left(m^2 s^{-1}\right)$	D_0 $\left(m^2 s^{-1}\right)$	k_I
0	$(1.0 \pm 0.9) \cdot 10^{-17}$	$(7.7 \pm 2.1) \cdot 10^{-17}$	0.13 ± 0.12
0.5			
6.0			

6

Microcapsule-functionalized Fibrous Materials

6.1 Formulation

A method for functionalizing regenerated polysaccharide fibers with particles on the micrometer and nanometer scale was developed in Paper V. Fiber matrices of cellulose, hydroxypropyl cellulose, chitosan, and alginate were employed, thus representing a wide range of fiber types. Additionally, both wet-spun continuous fiber filaments and solution-blown nonwoven textiles were produced. In these materials, functionalization by microcapsules of both monolithic and core-shell morphologies, as well as mesoporous silica nanoparticles, were achieved, thus demonstrating the versatility in choice of both the macroscopic fiber type and the choice of functionalization particles. Solution-blown cellulose nonwoven textiles functionalized by monolithic microcapsules were studied further in Paper VI and Paper VII, and will consequently be the main focus of this chapter.

The cellulose nonwoven materials used in Papers V-VII were produced using a technique called solution blowing [117], outlined schematically in Figure 6.1. Initially, a *dope solution* was prepared by dissolving microcrystalline cellulose in the ionic liquid 1-ethyl-3-methylimidazolium acetate (EMIMAc). This dope solution was then extruded through a spinneret containing capillaries of 220 μm diameter. The extruded fibers were coagulated in an aqueous coagulation bath and collected onto a rotating collector. In the air gap between the spinneret and coagulation bath, the extruded filaments were stretched by a parallel flow of compressed air. Functionalization of these textiles with nano- or microparticles is not straightforward but can be achieved by dispersing the particles in the dope solution prior to spinning. To enable this functionalization, there are a number of considerations that must be accounted for in the fiber spinning process.

Normally, dissolving pulp ($\approx$300 kg mol^{-1}) is used for preparing the dope solutions due to the superior mechanical properties it imparts to the prepared fibers. This results in a dope

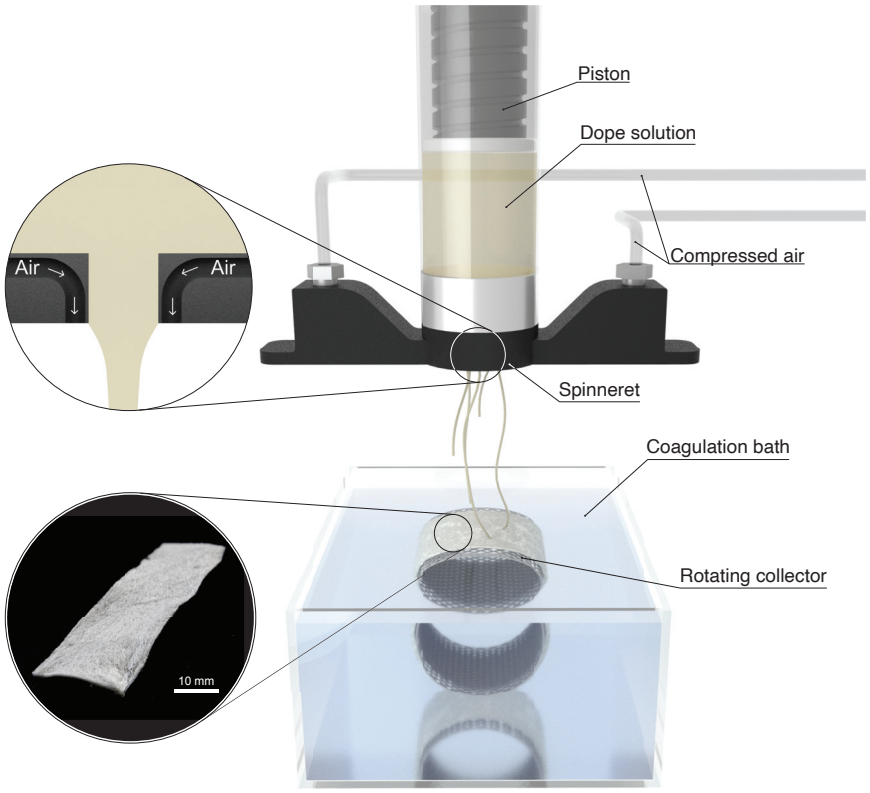

Figure 6.1: Illustration of the experimental setup used for preparing nonwovens by solution blowing, along with annotations of the different parts of the setup. The photograph in the inset shows a small piece of prepared nonwoven material.

solution with a high viscosity. For such a viscous dope solution to be spinnable, the solution blowing must be carried out while keeping the dope solution heated at up to 70 °C [117], which decreases its viscosity. However, biobased microcapsules are often sensitive to temperature due to their low glass transition temperatures, making the use of elevated temperatures during the solution blowing of microcapsule-functionalized fibers impossible. To decrease the viscosity of the solution, cosolvents such as dimethylsulfoxide or methylimidazole can be added [118]. Many of these EMIMAc/cosolvent mixtures tend to entirely disintegrate PLGA microcapsules. To circumvent these viscosity-related limitations, dope solutions were instead prepared with the lower molecular weight microcrystalline cellulose ($\approx$80 kg mol^{-1}) for microcapsule-functionalized fibers. This permitted spinning at room temperature, thus leaving the microcapsules intact during the processing. The resulting materials exhibited a uniform distribution of microcapsules throughout the fiber cross-section, with no observable fracturing or deformation of the microcapsules, as evidenced in Figure 6.2c. Additionally, the fluorescence micrograph in Figure 6.2c2 confirmed a high partitioning of the encapsulated pyrene towards the microcapsules.

6.2 Release of Actives

The study in Paper VI focused on evaluating the release rate-limiting properties imparted by microcapsules encapsulating pyrene, a model active substance, in a microcapsule-functionalized cellulose nonwoven. The release was compared to two forms of impregnation: surface and bulk impregnation, mimicking the loading processes commonly used in commercial products. Micrographs visualizing the difference in loading between these materials are shown in Figure 6.2. During surface impregnation, the fiber surface did not exhibit a uniform film of pyrene. Instead, discrete micrometer-sized areas with higher pyrene concentrations were found. Although surface heterogeneity was noticeable, pyrene could not be detected within the bulk of the fiber matrix. Conversely, bulk impregnation resulted in an even fluorescence intensity throughout the fiber cross-section, indicating a homogeneous loading in the entire fiber matrix rather than the heterogeneity observed for surface impregnation. It is important to note that cellulose possesses a slight autofluorescence in the same spectral region as pyrene, making precise quantification of partitioning challenging based solely on fluorescence micrographs.

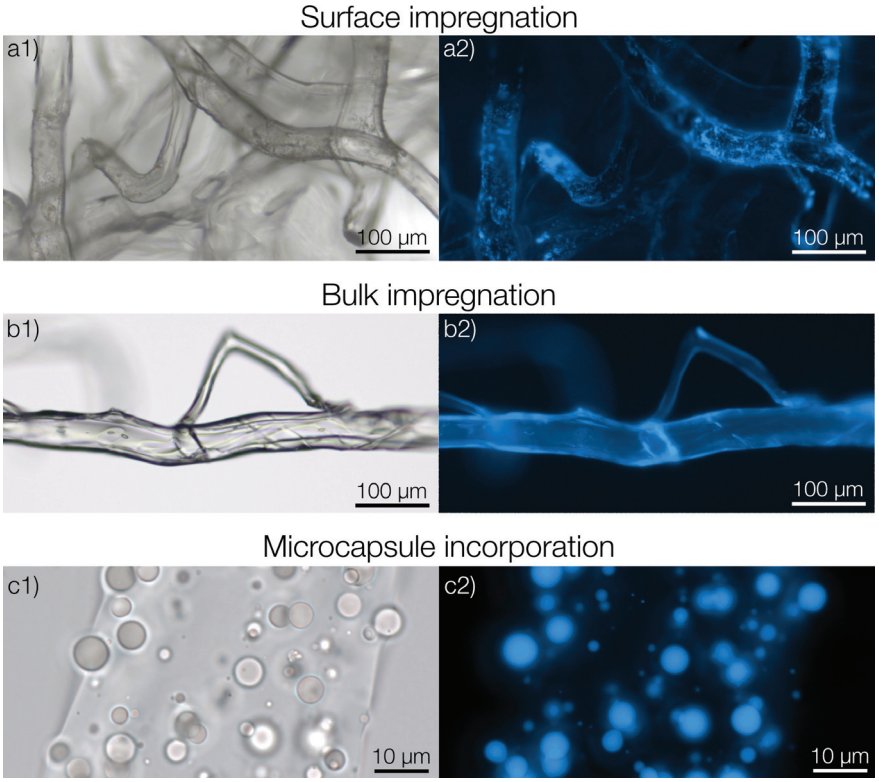

Figure 6.2: Three types of functionalized fibrous materials with pyrene as an active substance. a1) Optical micrograph of a fiber with a surface impregnation of pyrene. a2) Fluorescence micrograph of the same area. b1) and b2) Fibers with bulk impregnated pyrene. c1) and c2) Fibers with embedded microcapsules.

The release of pyrene from these three types of nonwovens was measured in an aqueous release medium, with the release profiles in Figure 6.3. A continuous decrease in release rate was observed when going from surface impregnation to bulk impregnation to encapsulation. Surface impregnation displayed a significant burst release of approximately 50% and achieved complete release within an hour. For the bulk impregnated material, no burst was observed, however, the release was still rapid and complete within 10 hours. With the help of microcapsules embedded in the fibers, the release time frame could be further extended to yield a complete release after more than 100 hours. To confirm the barrier properties introduced by the microcapsules, the release from microcapsules within the fiber matrix was

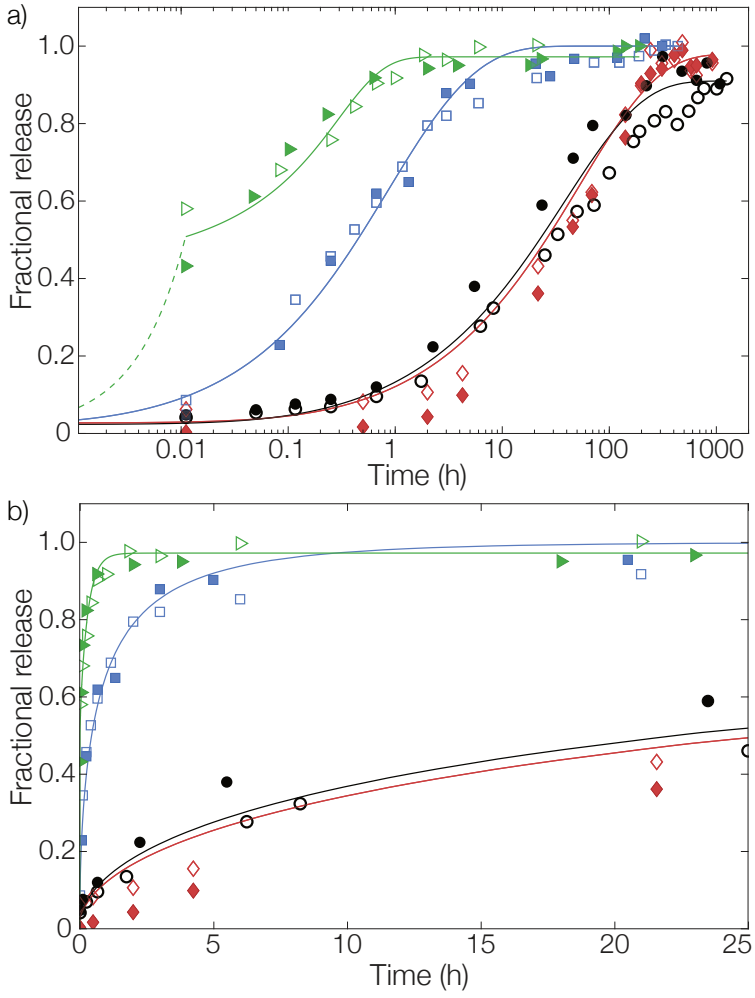

Figure 6.3: Fractional release from fibers with pyrene loaded by surface impregnation (▷▶), bulk impregnation (□■), and microencapsulation (◇◆). Release from microcapsules (without fibers) in aqueous suspension (○●) is shown as a comparison. Solid lines are fits to the diffusion models for the corresponding material geometries. In (a) the full release profile is shown on a logarithmic time scale, while in (b) the first 25 hours are shown on a linear time scale. All samples were studied in duplicates, as presented by filled and open symbols, and fitted lines are here shown as averages of individual fits to simplify visualization.

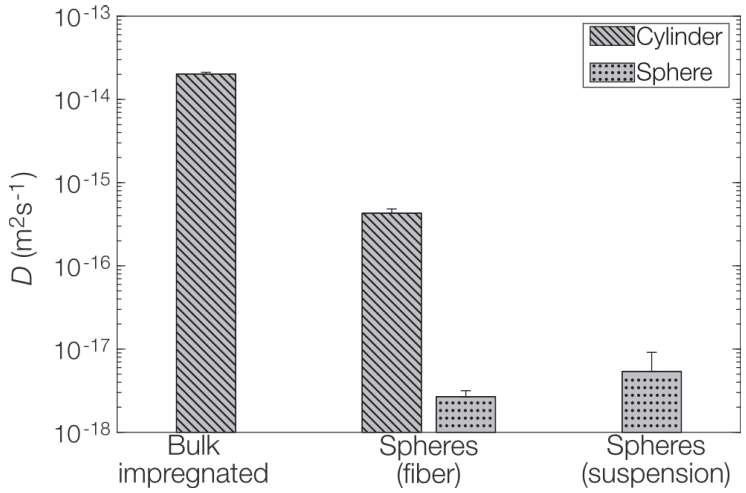

Figure 6.4: Fitted diffusion coefficients D from models based on both a cylinder (fiber) and a sphere (microcapsule).

compared to the release from microcapsules in an aqueous suspension. The release profiles demonstrated a high similarity, confirming the role of the microcapsules as a rate-limiting barrier.

A quantitative measure of the barrier properties added by the microcapsules was given by fitting release models based on Fickian diffusion in appropriate geometries (sphere, cylinder, or plane sheet) to the data. As discussed in the context of OCT-loaded microcapsules in Paper IV these models contain an effective diffusion coefficient that includes parameters such as (micro)porosity and interactions between active and matrix. For multi-compartment composite materials, such as the microcapsule-functionalized fibrous materials discussed here, another distinction is necessary. In these cases, the diffusion coefficient described by the models is an *apparent* diffusion coefficient, containing the collective impact of all compartments.

From the release model based on a cylindrical geometry (Equation 4.17) corresponding to the fiber dimensions, a reduction in apparent diffusion coefficient by nearly two orders of magnitude was found when comparing bulk impregnation to microcapsule-functionalization. Alternatively, considering only the microcapsules and fitting a model based on their spherical geometry revealed comparable diffusivities for both the microcapsule-functionalized material and microcapsules in aqueous suspension, despite the added diffusion layer of the fiber matrix surrounding the microcapsules. This further verified the rate-limiting properties added by the microcapsules.

6.3 Sustained Antimicrobial Activity

The OCT-loaded microcapsules, formulated and characterized in Paper IV, were incorporated into cellulose nonwovens in Paper VII following the approach outlined in Paper V and Paper VI. This functionalization aimed to enable a sustained release of antibacterial OCT from the nonwovens, and by extension long-term infection control. The developed material prototype was compared to cellulose nonwovens loaded via surface impregnation – a representation of commercially available materials. The infection control was evaluated against *S. aureus* as a model organism, because of its common occurrence in skin infections. A minimum loading concentration[‡] (MLC) of OCT against *S. aureus* in the impregnated materials was determined to be 150 µg OCT/g nonwoven. Therefore, the materials were loaded with approximately 1500 µg/g – both by impregnation and encapsulation.

The long-term antimicrobial effect of the materials was evaluated by a combination of two factors. First, the materials were exposed to an aqueous NaCl leaching medium with an ionic strength of 150 mM, mirroring that of wound exudate. Leaching occurred over 30 minutes, 1 day, and 1 week, aiming to study the remaining amount of OCT in the materials over time during a simulated exposure to wound exudate. After leaching, the materials were dried, inoculated with *S. aureus*, and their growth-inhibiting effect was evaluated during incubation for up to 68 hours. Any growth inhibition was measured by determining the number of viable bacteria, expressed as colony-forming units (CFU), in the samples after incubation. Initially, the materials were inoculated with 10^5 CFU. A decrease in the number of CFUs during incubation consequently indicated an antimicrobial effect.

As initially prepared, the impregnated material exhibited growth inhibition at all investigated incubation times, shown in Figure 6.5a. However, similar to the release of impregnated pyrene in Paper VI, the release of impregnated OCT was rapid and achieved a near-complete release within an hour. This is shown in the corresponding release measurement of OCT from the material in Figure 6.5a. After just 30 minutes of leaching, a significantly lower amount of OCT remained in the material which caused the release to only slightly exceed the MLC. This proximity to the MLC led to a weak growth inhibition of $\Delta\log(\text{CFU}) = -1$ at 68 hours of inhibition. As a result of the rapid release, the impregnated materials completely lost their antimicrobial efficacy after longer leaching times of 1 day and 1 week, respectively.

In contrast, nonwovens containing encapsulated OCT displayed an entirely different behavior. Instead of an immediate antimicrobial effect, a gradually increasing growth inhibition was observed, reaching a maximum ($\log \text{CFU} \leq 2$) after 68 hours of incubation. This trend was noted irrespective of the leaching time and originated from the slow and sustained release of OCT from the microcapsules. It is important to note that the release was far from complete within the experimental timeframe illustrated in Figure 6.5. In the encapsulated material,

[‡]The OCT loading in the nonwoven that is required to reach an antimicrobial effect, similar to the minimum inhibitory concentration (MIC).

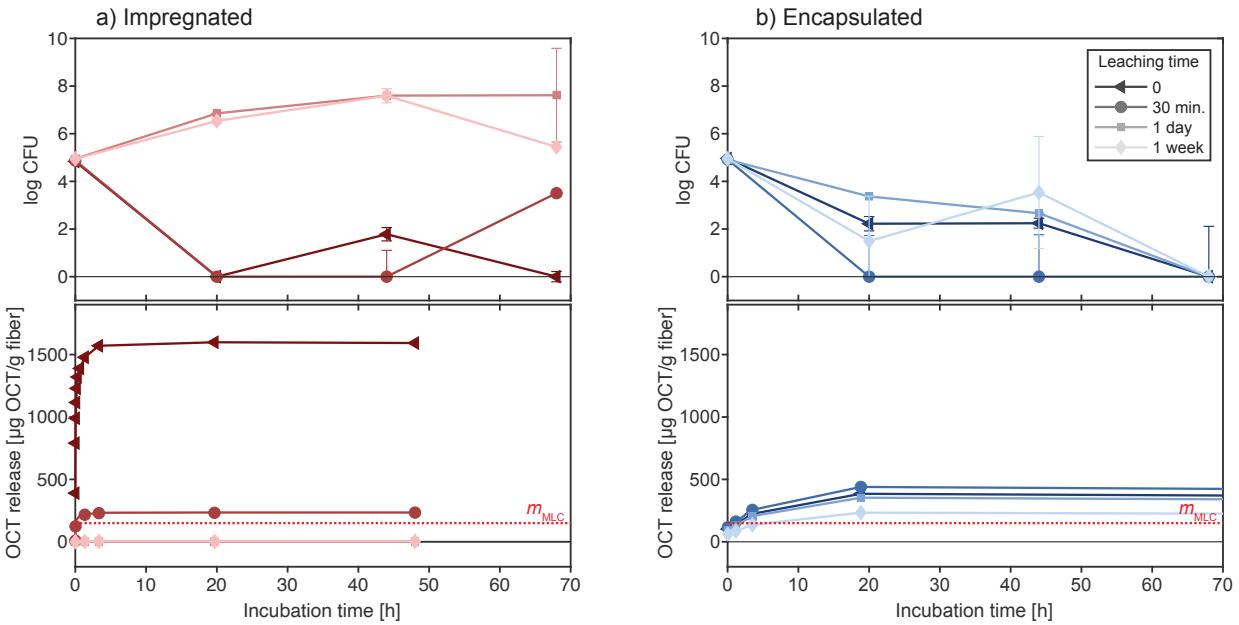

Figure 6.5: Long term antimicrobial effect for nonwovens containing a) impregnated and b) encapsulated OCT. The nonwovens have been subjected to various leaching times (0, 30 min., 1 day, and 1 week) after which the *S. aureus* growth inhibition has been evaluated as a function of incubation time. Below the growth inhibition curves, the corresponding release of OCT from the nonwoven samples is shown.

around 1500 µg OCT/g nonwoven was loaded, and only approximately one-third of the total loaded amount was released over 68 hours. Thus, the antimicrobial efficacy could potentially be extended far beyond the tested timeframe.

7

Concluding Remarks

In this thesis, a novel approach to functionalizing textile fibers with microcapsules was developed and evaluated. With the aim of enhancing the control over the release of actives from a macroscopic fibrous material, release rate-limiting microcapsules were immobilized within a regenerated cellulose fiber matrix. The initial objective was to understand the microencapsulation process and identify critical factors for controlling morphology, aiming to formulate microcapsules with controllable and predictable release properties. It was observed that the intermediate structure of microcapsules during formation – following internal phase separation – played a crucial role in determining the final morphological outcome of the formulation. Consequently, information about the phase behavior of the coacervating emulsion droplets can yield an improved capability of predicting and describing obtained microcapsule morphologies for which the classical thermodynamical equilibrium-based methods fail.

Through adjustment of the formulation parameters, systems capable of achieving both instantaneous triggered release and sustained release were successfully formulated. Utilizing stimuli-responsive polymer shells and incorporating morphological weak spots into the microcapsules facilitated the creation of stimuli-responsive release systems sensitive to both pH changes and UV light irradiation. By introducing a strong electrostatic interaction between the active and microcapsule matrix, a slow and sustained release of the active over several weeks to months was enabled. This interaction was verified to be the main mechanism controlling the restricted diffusivity of the active within the microcapsule.

Functionalization of a cellulose nonwoven material by microencapsulated actives of both hydrophobic and semi-hydrophilic nature was achieved. In both cases, the release rate-limiting properties of the microcapsules were retained after functionalization. To evaluate the implications of enabling a sustained release of actives from the developed material, long-term infection control was considered as a proof of concept. For this purpose, a cellulose nonwoven textile was functionalized with microcapsules encapsulating the antibacterial agent octenidine dihydrochloride (OCT). This material exhibited sustained antimicrobial efficacy

for at least one week. On the contrary, a material loaded with OCT through impregnation (mimicking commercially available alternatives) lost its efficacy within 30 minutes as a result of a rapid OCT release.

7.1 Future Outlook

The presented microcapsule functionalization shows great promise in the proof of concept for microbial infection control. However, further understanding of how different release profiles can be combined and how this would affect the required dose of active is required. For example, sustained and triggered release formulations could be combined to achieve both a rapid initial effect as well as a maintained effect over longer times. The versatility of the fiber functionalization technique, where microcapsules are dispersed in the dope solution during fiber spinning, allows for the utilization of several microcapsule types simultaneously within the same material.

While this work has demonstrated the potential of sustained release from the developed material, its applicability extends far beyond infection control. There is a wide range of commercially relevant cationic drugs, where encapsulation and release mechanisms similar to that of the studied OCT in this work would be anticipated. Additionally, alternate fiber types could be functionalized to, for example, enable a controlled release of pesticides or biocides from textiles utilized in agriculture or aquaculture. As evidenced by OCT, the encapsulation of highly water-soluble actives in monolithic microcapsules is possible. However, the current formulation route for preparing core-shell microcapsules, as used in this thesis, is confined to hydrophobic actives. Although more elaborate experimentally, there are methods available for formulating aqueous core microcapsules. Enhancing these formulation techniques to facilitate encapsulation and stimuli-responsive release of hydrophilic or semihydrophobic, often surface-active, actives would significantly broaden the possibilities of microcapsule functionalization, paving the way for a multitude of innovative applications.

Acknowledgments

The Swedish research council Formas is acknowledged for financial support.

This work would not have been possible without the help from many talented individuals:

My main supervisor, Lars Evenäs. Thank you for introducing me to the fantastic world of microencapsulation all those years ago. Your support has really helped me develop as a researcher.

My co-supervisor, Markus Andersson Trojer. Your enthusiasm and encouragement for my work has helped me develop and progress, especially in times of puzzling results.

My examiner, Martin Andersson. Thanks for your interest in my work.

Romain Bordes, your suggestions have given valuable input and new angles to the challenges of the project.

Jules, Jakob, Sofia, Matilda, Leyla and Erik. Your hard work during your thesis and/or project work has been invaluable. Many of the results in this thesis would not have been included without your help.

All co-authors, thanks for rewarding collaborations and fruitful discussions.

Members of *SynCap*, our discussions have improved my work significantly and helped me see the bigger picture of my research.

Everyone at the Applied Chemistry division. Thanks for creating such a nice atmosphere both in and out of work. Having colleagues like you have made these past years a delight!

Finally, friends and family for your support during these years. Especially Elin for your constant love and support. Thank you for always being there for me.

Viktor Eriksson
Mölndal, November 2023

References

(1) Lindblad, W. J. *The International Journal of Lower Extremity Wounds* **2008**, *7*, 75–81.
(2) Dafforn, K. A.; Lewis, J. A.; Johnston, E. L. *Marine Pollution Bulletin* **2011**, *62*, 453–465.
(3) Ligon, B. L. In *Seminars in Pediatric Infectious Diseases*, 2004; Vol. 15, pp 52–57.
(4) Clark, E. A.; Sterritt, R. M.; Lester, J. N. *Environmental Science & Technology* **1988**, *22*, 600–604.
(5) Evans, S.; Leksono, T.; McKinnell, P. *Marine Pollution Bulletin* **1995**, *30*, 14–21.
(6) Gullberg, E.; Cao, S.; Berg, O. G.; Ilbäck, C.; Sandegren, L.; Hughes, D.; Andersson, D. I. *PLoS Pathogens* **2011**, *7*, e1002158.
(7) Interagency Coordination Group on Antimicrobial Resistance *No time to wait: securing the future from drug-resistant infections*; 2019.
(8) European Commission *EU Action Plan: 'Towards Zero Pollution for Air, Water and Soil'*; 2021.
(9) Cedergreen, N. *PloS One* **2014**, *9*, e96580.
(10) Mishra, M. K. In *Kirk-Othmer Encyclopedia of Chemical Technology*; John Wiley & Sons, Ltd: 2019, pp 1–35.
(11) Trojer, M. A.; Nordstierna, L.; Nordin, M.; Nydén, M.; Holmberg, K. *Physical Chemistry Chemical Physics* **2013**, *15*, 17727–17741.
(12) Esser-Kahn, A. P.; Odom, S. A.; Sottos, N. R.; White, S. R.; Moore, J. S. *Macromolecules* **2011**, *44*, 5539–5553.
(13) Bergek, J.; Trojer, M. A.; Uhr, H.; Nordstierna, L. *Journal of Controlled Release* **2016**, *225*, 31–39.
(14) Paul, R., *High Performance Technical Textiles*; John Wiley & Sons: 2019.
(15) Sandin, G.; Roos, S.; Johansson, M. Environmental impact of textile fibers–what we know and what we don't know: Fiber Bible part 2, 2019.
(16) Klemm, D.; Heublein, B.; Fink, H.-P.; Bohn, A. *Angewandte Chemie International Edition* **2005**, *44*, 3358–3393.
(17) Kellie, G., *Advances in Technical Nonwovens*; Woodhead Publishing: 2016.
(18) Javaid, S.; Mahmood, A.; Nasir, H.; Iqbal, M.; Ahmed, N.; Ahmad, N. M. *Polymers* **2022**, *14*, 2540.
(19) Liu, Z.; Xu, M.; Wang, Q.; Li, B. *Cellulose* **2017**, *24*, 4069–4081.
(20) Zhang, Y.; Xia, X.; Ma, K.; Xia, G.; Wu, M.; Cheung, Y. H.; Yu, H.; Zou, B.; Zhang, X.; Farha, O. K.; Xin, J. H. *Advanced Functional Materials* **2023**, 2301607.

(21) Naeimirad, M.; Zadhoush, A.; Kotek, R.; Esmaeely Neisiany, R.; Nouri Khorasani, S.; Ramakrishna, S. *Journal of Applied Polymer Science* **2018**, *135*, 46265.
(22) Alay, S.; Alkan, C.; Göde, F. *Thermochimica Acta* **2011**, *518*, 1–8.
(23) Monllor, P.; Bonet, M. A.; Cases, F. *European Polymer Journal* **2007**, *43*, 2481–2490.
(24) Crespy, D.; Friedemann, K.; Popa, A.-M. *Macromolecular Rapid Communications* **2012**, *33*, 1978–1995.
(25) Reinke, J.; Sorg, H. *European Surgical Research* **2012**, *49*, 35–43.
(26) Landén, N. X.; Li, D.; Ståhle, M. *Cellular and Molecular Life Sciences* **2016**, *73*, 3861–3885.
(27) Raeder, K.; Jachan, D. E.; Müller-Werdan, U.; Lahmann, N. A. *International Wound Journal* **2020**, *17*, 1128–1134.
(28) Rahim, K.; Saleha, S.; Zhu, X.; Huo, L.; Basit, A.; Franco, O. L. *Microbial Ecology* **2017**, *73*, 710–721.
(29) Malone, M.; Bjarnsholt, T.; McBain, A. J.; James, G. A.; Stoodley, P.; Leaper, D.; Tachi, M.; Schultz, G.; Swanson, T.; Wolcott, R. D. *Journal of Wound Care* **2017**, *26*, 20–25.
(30) McShan, D.; Ray, P. C.; Yu, H. *Journal of Food and Drug Analysis* **2014**, *22*, 116–127.
(31) Khansa, I.; Schoenbrunner, A. R.; Kraft, C. T.; Janis, J. E. *Plastic and Reconstructive Surgery Global Open* **2019**, *7*.
(32) Kalantari, K.; Mostafavi, E.; Afifi, A. M.; Izadiyan, Z.; Jahangirian, H.; Rafiee-Moghaddam, R.; Webster, T. J. *Nanoscale* **2020**, *12*, 2268–2291.
(33) Husmark, J.; Morgner, B.; Susilo, Y. B.; Wiegand, C. *Journal of Wound Care* **2022**, *31*, 560–570.
(34) Malone, M.; Nygren, E.; Hamberg, T.; Radzieta, M.; Jensen, S. O. *International Wound Journal* **2023**, 1–16.
(35) Jennings, M. C.; Minbiole, K. P.; Wuest, W. M. *ACS Infectious Diseases* **2015**, *1*, 288–303.
(36) Alkhalifa, S.; Jennings, M. C.; Granata, D.; Klein, M.; Wuest, W. M.; Minbiole, K. P.; Carnevale, V. *ChemBioChem* **2020**, *21*, 1510–1516.
(37) Barros, A. C.; Melo, L. F.; Pereira, A. *Frontiers in Microbiology* **2022**, *13*, 842414.
(38) Vasilev, K. *Coatings* **2019**, *9*, 654.
(39) Roy, D.; Knapp, J. S.; Guthrie, J. T.; Perrier, S. *Biomacromolecules* **2008**, *9*, 91–99.
(40) Hadjesfandiari, N.; Yu, K.; Mei, Y.; Kizhakkedathu, J. N. *Journal of Materials Chemistry B* **2014**, *2*, 4968–4978.
(41) Hübner, N.-O.; Siebert, J.; Kramer, A. *Skin Pharmacology and Physiology* **2010**, *23*, 244–258.
(42) Koburger, T.; Hübner, N.-O.; Braun, M.; Siebert, J.; Kramer, A. *Journal of Antimicrobial Chemotherapy* **2010**, *65*, 1712–1719.
(43) Malanovic, N.; Ön, A.; Pabst, G.; Zellner, A.; Lohner, K. *International Journal of Antimicrobial Agents* **2020**, *56*, 106146.
(44) Gilbert, P.; McBain, A. J. *Clinical Microbiology Reviews* **2003**, *16*, 189–208.

(45) Bysell, H.; Månsson, R.; Hansson, P.; Malmsten, M. *Advanced Drug Delivery Reviews* **2011**, *63*, 1172–1185.
(46) Lengyel, M.; Kállai-Szabó, N.; Antal, V.; Laki, A. J.; Antal, I. *Scientia Pharmaceutica* **2019**, *87*, 20.
(47) White, A. L.; Langton, C.; Wille, M.-L.; Hitchcock, J.; Cayre, O. J.; Biggs, S.; Blakey, I.; Whittaker, A. K.; Rose, S.; Puttick, S. *Journal of Colloid and Interface Science* **2019**, *554*, 444–452.
(48) Trojer, M. A.; Nordstierna, L.; Bergek, J.; Blanck, H.; Holmberg, K.; Nydén, M. *Advances in Colloid and Interface Science* **2015**, *222*, 18–43.
(49) Zhao, Y.; Zhang, W.; Liao, L.-P.; Wang, S.-J.; Li, W.-J. *Applied Surface Science* **2012**, *258*, 1915–1918.
(50) Rule, J. D.; Sottos, N. R.; White, S. R. *Polymer* **2007**, *48*, 3520–3529.
(51) Augustin, M. A.; Hemar, Y. *Chemical Society Reviews* **2009**, *38*, 902–912.
(52) Elsner, J.; Berdicevsky, I.; Zilberman, M. *Acta Biomaterialia* **2011**, *7*, 325–336.
(53) Comiskey, B.; Albert, J. D.; Yoshizawa, H.; Jacobson, J. *Nature* **1998**, *394*, 253–255.
(54) Tong, W.; Song, X.; Gao, C. *Chemical Society Reviews* **2012**, *41*, 6103–6124.
(55) Städler, B.; Chandrawati, R.; Price, A. D.; Chong, S.-F.; Breheney, K.; Postma, A.; Connal, L. A.; Zelikin, A. N.; Caruso, F. *Angewandte Chemie International Edition* **2009**, *48*, 4359–4362.
(56) Fanger, G. O. In *Microencapsulation: Processes and Applications*, Vandegaer, J. E., Ed.; Springer US: Boston, MA, 1974, pp 1–20.
(57) Loxley, A.; Vincent, B. *Journal of Colloid and Interface Science* **1998**, *208*, 49–62.
(58) Long, Y.; York, D.; Zhang, Z.; Preece, J. A. *Journal of Materials Chemistry* **2009**, *19*, 6882–6887.
(59) Atkin, R.; Davies, P.; Hardy, J.; Vincent, B. *Macromolecules* **2004**, *37*, 7979–7985.
(60) Uchida, T.; Yoshida, K.; Goto, S. *Journal of Microencapsulation* **1996**, *13*, 219–228.
(61) Meng, F.; Ma, G.; Liu, Y.; Qiu, W.; Su, Z. *Colloids and Surfaces B: Biointerfaces* **2004**, *33*, 177–183.
(62) Nordstierna, L.; Movahedi, A.; Nydén, M. *Journal of Dispersion Science and Technology* **2011**, *32*, 310–311.
(63) Bergek, J.; Trojer, M. A.; Mok, A.; Nordstierna, L. *Colloids and Surfaces A: Physicochemical and Engineering Aspects* **2014**, *458*, 155–167.
(64) Torza, S.; Mason, S. G. *Journal of Colloid and Interface Science* **1970**, *33*, 67–83.
(65) Sundberg, D. C.; Casassa, A. P.; Pantazopoulos, J.; Muscato, M. R.; Kronberg, B.; Berg, J. *Journal of Applied Polymer Science* **1990**, *41*, 1425–1442.
(66) Tang, S.; Yourdkhani, M.; Possanza Casey, C. M.; Sottos, N. R.; White, S. R.; Moore, J. S. *ACS Applied Materials & Interfaces* **2017**, *9*, 20115–20123.
(67) Pekarek, K. J.; Jacob, J. S.; Mathiowitz, E. *Nature* **1994**, *367*, 258–260.
(68) Trongsatitkul, T.; Budhlall, B. M. *Langmuir* **2011**, *27*, 13468–13480.
(69) Esteki, B.; Masoomi, M.; Moosazadeh, M.; Yoo, C. *Langmuir* **2023**, *39*, 4943–4958.

(70) Berry, J. D.; Neeson, M. J.; Dagastine, R. R.; Chan, D. Y.; Tabor, R. F. *Journal of Colloid and Interface Science* **2015**, *454*, 226–237.
(71) Van Oss, C.; Good, R.; Chaudhury, M. *Langmuir* **1988**, *4*, 884–891.
(72) Berkland, C.; Kipper, M. J.; Narasimhan, B.; Kim, K. K.; Pack, D. W. *Journal of Controlled Release* **2004**, *94*, 129–141.
(73) Thomas, P.; Padmaja, T.; Kulkarni, M. *Journal of Controlled Release* **1997**, *43*, 273–281.
(74) Fu, J.; Sun, F.; Liu, W.; Liu, Y.; Gedam, M.; Hu, Q.; Fridley, C.; Quigley, H. A.; Hanes, J.; Pitha, I. *Molecular Pharmaceutics* **2016**, *13*, 2987–2995.
(75) Erdmann, L.; Uhrich, K. *Biomaterials* **2000**, *21*, 1941–1946.
(76) Schmeltzer, R. C.; Anastasiou, T. J.; Uhrich, K. E. *Polymer Bulletin* **2003**, *49*, 441–448.
(77) Whitaker-Brothers, K.; Uhrich, K. *Journal of Biomedical Materials Research Part A* **2006**, *76*, 470–479.
(78) Carbone, A. L.; Uhrich, K. E. *Macromolecular Rapid Communications* **2009**, *30*, 1021–1026.
(79) Schneider, L. A.; Korber, A.; Grabbe, S.; Dissemond, J. *Archives of Dermatological Research* **2007**, *298*, 413–420.
(80) Percival, S. L.; McCarty, S.; Hunt, J. A.; Woods, E. J. *Wound Repair and Regeneration* **2014**, *22*, 174–186.
(81) Erdmann, L.; Macedo, B.; Uhrich, K. *Biomaterials* **2000**, *21*, 2507–2512.
(82) Aso, C.; Tagami, S. *Journal of Polymer Science Part B: Polymer Letters* **1967**, *5*, 217–220.
(83) Ito, H.; Willson, C. G. *Polymer Engineering & Science* **1983**, *23*, 1012–1018.
(84) Ito, H.; Willson, C. G. In *Polymers in Electronics*; ACS Publications: 1984, pp 11–23.
(85) DiLauro, A. M.; Abbaspourrad, A.; Weitz, D. A.; Phillips, S. T. *Macromolecules* **2013**, *46*, 3309–3313.
(86) Tang, S.; Tang, L.; Lu, X.; Liu, H.; Moore, J. S. *Journal of the American Chemical Society* **2018**, *140*, 94–97.
(87) Kaitz, J. A.; Lee, O. P.; Moore, J. S. *MRS Communications* **2015**, *5*, 191–204.
(88) Wang, F.; Diesendruck, C. E. *Macromolecular Rapid Communications* **2018**, *39*, 1700519.
(89) Harrison, T. S.; Goa, K. L. *CNS drugs* **2004**, *18*, 113–132.
(90) Su, Y.; Zhang, B.; Sun, R.; Liu, W.; Zhu, Q.; Zhang, X.; Wang, R.; Chen, C. *Drug Delivery* **2021**, *28*, 1397–1418.
(91) Anderson, J. M.; Shive, M. S. *Advanced Drug Delivery Reviews* **1997**, *28*, 5–24.
(92) Babu, R. P.; O'connor, K.; Seeram, R. *Progress in Biomaterials* **2013**, *2*, 1–16.
(93) Fredenberg, S.; Wahlgren, M.; Reslow, M.; Axelsson, A. *International Journal of Pharmaceutics* **2011**, *415*, 34–52.
(94) Von Burkersroda, F.; Schedl, L.; Göpferich, A. *Biomaterials* **2002**, *23*, 4221–4231.
(95) Li, L.; Schwendeman, S. P. *Journal of Controlled Release* **2005**, *101*, 163–173.

(96) Gu, B.; Sun, X.; Papadimitrakopoulos, F.; Burgess, D. J. *Journal of Controlled Release* **2016**, *228*, 170–178.
(97) Gasmi, H.; Danede, F.; Siepmann, J.; Siepmann, F. *Journal of Controlled Release* **2015**, *213*, 120–127.
(98) Köhler, A. *Zeitschrift für Wissenschaftliche Mikroskopie und für Mikroskopische Technik* **1893**, *10*, 433–440.
(99) Kubitscheck, U., *Fluorescence Microscopy: From Principles to Biological Applications.* John Wiley & Sons, Incorporated: 2017.
(100) Lakowicz, J. R., *Principles of Fluorescence Spectroscopy*; Springer: 2006.
(101) Xu, R., *Particle characterization: light scattering methods*; Springer Science & Business Media: 2001; Vol. 13.
(102) Larkin, P., *Infrared and Raman Spectroscopy: Principles and Spectral Interpretation*; Elsevier: 2017.
(103) Takka, S. *Il Farmaco* **2003**, *58*, 1051–1056.
(104) Coughlan, D.; Corrigan, O. *International Journal of Pharmaceutics* **2006**, *313*, 163–174.
(105) Gibaldi, M.; Feldman, S. *Journal of Pharmaceutical Sciences* **1967**, *56*, 1238–1242.
(106) Crank, J., *The Mathematics of Diffusion*; Oxford University Press: 1979.
(107) Packer, K.; Rees, C. *Journal of Colloid and Interface Science* **1972**, *40*, 206–218.
(108) Huang, X.; Brazel, C. S. *Journal of Controlled Release* **2001**, *73*, 121–136.
(109) Versypt, A. N. F.; Pack, D. W.; Braatz, R. D. *Journal of Controlled Release* **2013**, *165*, 29–37.
(110) Pitt, C. G.; Zhong-wei, G. *Journal of Controlled Release* **1987**, *4*, 283–292.
(111) Antheunis, H.; van der Meer, J.-C.; de Geus, M.; Heise, A.; Koning, C. E. *Biomacromolecules* **2010**, *11*, 1118–1124.
(112) Tavera, E. M.; Kadali, S. B.; Bagaria, H. G.; Liu, A. W.; Wong, M. S. *AIChE Journal* **2009**, *55*, 2950–2965.
(113) Andersson Trojer, M.; Holmberg, K.; Nydén, M. *Langmuir* **2012**, *28*, 4047–4050.
(114) Trojer, M. A.; Li, Y.; Abrahamsson, C.; Mohamed, A.; Eastoe, J.; Holmberg, K.; Nydén, M. *Soft Matter* **2013**, *9*, 1468–1477.
(115) Klaue, A.; Maraldi, M.; Piviali, C.; Moscatelli, D.; Morbidelli, M. *European Polymer Journal* **2020**, *138*, 109987.
(116) Blasi, P.; D'Souza, S. S.; Selmin, F.; DeLuca, P. P. *Journal of Controlled Release* **2005**, *108*, 1–9.
(117) Jedvert, K.; Idström, A.; Köhnke, T.; Alkhagen, M. *Journal of Applied Polymer Science* **2020**, *137*, 48339.
(118) Olsson, C.; Hedlund, A.; Idström, A.; Westman, G. *Journal of Materials Science* **2014**, *49*, 3423–3433.